

**Evaluation of Concrete Pavements
with Materials-Related Distress**

Final Report

Principal Investigator

Dr. Lawrence Sutter, Professor
(906) 487-2268
llsutter@mtu.edu

Michigan Tech Transportation Institute
Michigan Technological University
1400 Townsend Drive
Houghton, Michigan 49931

March 2, 2010

Michigan Tech
Transportation Institute

Partnering for the future of transportation.

Technical Report Documentation Page

1. Report No. RC-1533	2. Government Accession No.	3. MDOT Project Manager David Smiley	
4. Title and Subtitle Evaluation of Concrete Pavements with Materials-Related Distress		5. Report Date 3/02/2010	
		6. Performing Organization Code	
7. Author(s) Lawrence Sutter, Thomas VanDam, Karl Peterson		8. Performing Org. Report No.	
9. Performing Organization Name and Address Michigan Tech Transportation Institute Michigan Technological University 1400 Townsend Dr. Houghton, Michigan 49931		10. Work Unit No. (TRAIS)	
		11. Contract No. 2003-0063	
		11(a). Authorization No. Z20/R1	
12. Sponsoring Agency Name and Address MDOT Construction and Technology Division 8885 Ricks Road P.O. Box 30049 Lansing, MI 48909		13. Type of Report & Period Covered	
		14. Sponsoring Agency Code	
15. Supplementary Notes			
16. Abstract An evaluation of cores sampled from six concrete pavements was performed. Factors contributing to pavement distress observed in the field were determined, including expansive alkali-silica reactivity and freeze-thaw deterioration related to poor entrained air-void parameters. A laboratory study to investigate the role of alkali-silica reactivity through accelerated mortar bar and concrete prism testing was proposed.			
17. Key Words Alkali-Silica Reaction, Freeze-Thaw Durability		18. Distribution Statement No restrictions. This document is available to the public through the Michigan Department of Transportation.	
19. Security Classification - report	20. Security Classification - page	21. No. of Pages 69 and CD Appendix	22. Price

Disclaimer

The contents of this report reflect the views of the author/principal investigator who is responsible for the facts and accuracy of the data presented herein. The contents do not necessarily reflect the views or policies of the Michigan Department of Transportation or the Federal Highway Administration. This report does not constitute a standard, specification, or regulation.

Acknowledgements

This report was completed with support from the Michigan Department of Transportation. Technical editing was performed by Pamela Hannon.

TABLE OF CONTENTS

List of Figures	v
List of Tables	viii
Executive Summary	1
Introduction.....	3
Project Background.....	3
Objective.....	5
Scope.....	7
Methodology	11
Discussion of Results.....	13
WB I-696, I-94 Interchange, Roseville.....	15
SB M-5, 12 Mile Rd. to 14 Mile Rd., Novi	29
EB M-59, Hayes Rd. to Romeo Plank Rd., Clinton Township	35
EB M-14, I-94 to Huron River.....	41
NB US-23, Strategic Highway Research Program (SHRP) Section 19.....	45
SB US-23, MDOT Aggregate Test Site Section B.....	51
Summary	57
Discussion and Conclusions	59
Recommendations for Implementation & Further Research	61
List of Acronyms, Abbreviations and Symbols.....	65
Bibliography	67
Appendix.....	69

LIST OF FIGURES

Figure 1: Photo of I-696 median lane, with no visible distress at pavement surface. 16

Figure 2: Photo of I-696 median lane, with no visible distress at pavement surface. 16

Figure 3: Photo of I-696 outside lane, with cracks visible at pavement surface. 17

Figure 4: Photo of I-696, outside lane, deterioration at joints mostly covered by cold-patch material. 17

Figure 5: Slabs to represent cross section through core C, mid-panel, MTU ID 696-11, outside lane, WB I-696, after treatment to enhance air voids and cracks, tic marks every inch..... 18

Figure 6: Slabs to represent cross section through core B, at joint, MTU ID 696-10, outside lane, WB I-696, after treatment to enhance air voids and cracks, tic marks every inch. 19

Figure 7: Slabs to represent cross section through core A, at joint, MTU ID 696-09, outside lane, WB I-696, after treatment to enhance air voids and cracks, tic marks every inch..... 20

Figure 8: Epifluorescent mode (left) and transmitted light (right) images at transition between zone of abundant entrained air and zone without entrained air at a depth of approximately 3 inches (75 mm). Example from thin section prepared from core taken from I-696, outside lane, away from joint, MTU ID 696-03..... 21

Figure 9: Overview of sodium cobaltinitrite stained slabs from I-696 sites. The slabs represent full cross-sections through the pavement, with tic marks along the left hand side at one inch intervals..... 22

Figure 10: Alkali silica reaction in fine aggregate and associated cracking, before and after sodium cobaltinitrite stain, polished slab from I-696, constructed in 1995, median lane, away from transverse joint, top half of core D, MTU ID 696-03. 23

Figure 11: Alkali silica reaction in fine aggregate and associated cracking, before and after sodium cobaltinitrite stain, polished slab from I-696, constructed in 1995, median lane, away from transverse joint, top half of core D, MTU ID 696-03. 24

Figure 12: Slab representing cross section through top half of pavement, after treatment to enhance air voids and cracks, WB I-696, constructed in 1995, median lane, at transverse joint, core A, MTU ID 696-06, tic marks every half inch. 25

Figure 13: Slab representing cross section through top half of pavement, after treatment to enhance air voids and cracks, WB I-696, constructed in 1995, median lane, away from transverse joint, core D, MTU ID 696-03, tic marks every half inch.26

Figure 14: Example of chert particle exhibiting deleterious alkali-silica reaction in thin section prepared from core from I-696, constructed in 1995, median lane, away from transverse joint, MTU ID 696-03. From top to bottom: transmitted light, crossed-polars, and epifluorescent mode images.....27

Figure 15: Thin sections arranged in their original spatial context to show the longitudinal joint in cross-section. Voids and cracks in the inverted UV fluorescent image appear dark. Coarse sand particles observed at the pavement surface and filling the joint were blended with the epoxy to conserve epoxy during impregnation of the core segment.30

Figure 16: Overview of sodium cobaltinitrite stained slabs from all sites, excluding I-696. The slabs represent full cross-sections through the pavement, with tic marks along the left hand side at one inch intervals.....31

Figure 17: Successive close-up images of alkali silica reaction in fine aggregate and associated cracking near pavement surface, after sodium cobaltinitrite stain, polished slab from SB M-5, outside lane, at transverse joint, core B, MTU ID M5-05.32

Figure 18: Examples of cement paste both without (left) and with (right) fly ash spheres. Left-hand side image from core M-5, outside lane, at transverse joint, MTU ID M5-05. Right-hand side image from core M-5, median lane, away from joint, MTU ID M5-02. From top to bottom: transmitted light, crossed-polars, and epifluorescent mode images.....33

Figure 19: Alkali silica reaction in fine aggregate and associated cracking, before and after sodium cobaltinitrite stain, polished slab from top half of M-59, outside lane, away from transverse joint, core C, MTU ID M59-02.36

Figure 20: Alkali silica reaction in fine aggregate and associated cracking, before and after sodium cobaltinitrite stain, polished slab from top half of M-59, outside lane, away from transverse joint, core C, MTU ID M59-02.37

Figure 21: Slab representing cross section through top half of pavement, after treatment to enhance air voids and cracks, EB M-59, outside lane, away from transverse joint, core C, MTU ID M59-02, tic marks every half inch.....38

Figure 22: Example of chert particle exhibiting deleterious alkali-silica reaction, from thin section prepared from core from M-59, outside lane at joint, MTU ID M59-01. From top to bottom: transmitted light, crossed-polars, and epifluorescent mode images. 39

Figure 23: Alkali silica reaction in fine aggregate, with absence of cracking, before and after sodium cobaltinitrite stain, polished slab from top half of M-14, core B, at-joint, MTU ID M14-02. 42

Figure 24: Alkali silica reaction in fine aggregate, with absence of cracking, before and after sodium cobaltinitrite stain, polished slab from top half of M-14, core B, at-joint, MTU ID M14-02. 43

Figure 25: Carbonate dust in cement paste fraction in thin section prepared from core from M-14, away from joint, MTU ID M14-03. From top to bottom: transmitted light, crossed-polars, and epifluorescent mode images. 44

Figure 26: Alkali silica reaction in fine aggregate and associated cracking, before and after sodium cobaltinitrite stain, polished slab from top half of US-23, Section 19, at-joint, MTU ID US23-05. 46

Figure 27: Example of chert particle, and brown siltstone particle, both with minor cracking associated with alkali-silica reaction, from thin section prepared from core from US23, Section 19, away from joint, MTU ID US23-03. From top to bottom: transmitted light, crossed-polars, and epifluorescent mode images. 47

Figure 28: Close-up example of chert particle, and brown siltstone particle from previous figure, both with minor cracking associated with alkali-silica reaction, from thin section prepared from core from US23, Section 19, away from joint, MTU ID US23-03. From top to bottom: transmitted light, crossed-polars, and epifluorescent mode images. 48

Figure 29: Carbonate dust in cement paste fraction in thin section prepared from core from US23, Section 19, away from joint, MTU ID US23-03. From top to bottom: transmitted light, crossed-polars, and epifluorescent mode images. 49

Figure 30: Overview of US-23, Section B test site. 52

Figure 32: Polished slabs to represent cross-section through core MTU US23-07. 53

Figure 33: Polished slabs to represent cross-section through core MTU US23-06. 54

Figure 34: Alkali silica reaction in fine aggregate and associated cracking, before and after sodium cobaltinitrite stain, polished slab from top half of US-23, Section B, mid-panel, MTU ID US23-06.....55

Figure 35: Fly ash in cement paste fraction in thin section prepared from core from US23, Section B at longitudinal joint, MTU ID US23-07. From top to bottom: transmitted light, crossed-polars, and epifluorescent mode images.....56

LIST OF TABLES

Table 1: Summary of key materials-related distresses in concrete pavements..... 4

Table 2: Summary of coring sites. 8

Table 3: List of cores. 9

Table 4: Equivalent *w/c* ratio, as compared to 28-day cured mortar standards. 13

Table 5: ASTM C 457 air-void system parameters. 14

Table 6: Summary of distress mechanisms observed in test sites. 57

EXECUTIVE SUMMARY

Over the past 20 years materials related distress (MRD) has shortened the service life of several concrete pavement projects within the greater Metro Detroit area. Generally, the observed deterioration has started with cracking and crumbling at the joints, eventually progressing further into the slab. The 1992 US-23 project in Genesee County, (CS 25031-30798A) which was reconstructed in 2005, is an example of this destructive process. Recent research studies focusing on MRD (MDOT Research Reports RC1443 and RC1425) confirmed that alkali-silica reactivity, (ASR) paste freeze-thaw damage, and aggregate freeze-thaw damage exist within Michigan's concrete pavements. For example, past research efforts into ASR found that the chert fraction of the fine aggregate used produced damage in a number of the investigated pavement sections. Often, slag coarse aggregate and Class C fly ash were used together in situations where deleterious ASR occurred. With regards to aggregate freeze-thaw damage, it appears only in older projects constructed prior to MDOT adopting more strict aggregate freeze-thaw criteria in the 1970s and 1980s, which has effectively corrected the problem.

To further investigate the MRD problem, six pavement sections representing a range of MRD severities were selected for this study. Pavement sections were visited, and cores collected for further examination at the Michigan Technological University Transportation Materials Research Center in an effort to interpret factors contributing to MRD. Microscopic examination of samples prepared from the cores showed that ASR within the fine aggregate fraction, and freeze-thaw damage to the hardened cement paste were both contributing factors.

Strategies for the prevention of ASR in new construction are presented, including the placement of limitations on the maximum alkali content of the cementitious materials, the substitution of portland cement by supplementary cementitious materials (SCMs) including fly ash, ground granulated blast furnace slag, (GGBFS) and silica fume, and the incorporation of predictive tests such as the accelerated mortar bar test (AMBT) to assess the potential for ASR. Possible shortcomings to these ASR prevention strategies are discussed, including the restricted availability in Michigan of low-alkali content portland cements and fly ash, and a limited understanding of the effectiveness of current MDOT SCM maximum replacement limits for the mitigation of ASR.

Recommendations are made for additional research to define the unique post-construction, interaction relationships that occur amongst commonly used Michigan materials for concrete pavement to assure their selection produces a long-term, durable concrete mixture. These materials include fine aggregate susceptible to forming expansive ASR, blast furnace slag coarse aggregate, Class C fly ash, and high-alkali cements. The paste freeze-thaw MRD issues identified in this study are currently under investigation by Michigan Tech under a separate MDOT project titled "Impact of Hydrated Cement Paste Quality and Entrained Air-Void System on the Durability of Concrete" and are not addressed within this report.

THIS PAGE INTENTIONALLY LEFT BLANK

INTRODUCTION

Project Background

MRD is a general classification for durability issues in portland cement concrete (PCC) that are related to the materials used in construction, as compared to distress initiated by excessive loading or other design considerations. Although MRD has always been an issue with some PCC pavement structures, the recent trend towards utilization of a wide-range of materials has led to an increased occurrence of these types of distresses. Although the specific type of distresses may vary geographically, it is clear that a better understanding of these types of pavement failures is an important starting point for pavements to have improved service lives.

Whether a concrete pavement will be affected by MRD is a function of many factors, including the constituent materials used (aggregate, cement, additives, etc.) the location (maritime or inland), the climatic conditions (temperature, moisture) and the presence of external agents (such as roadway deicing chemicals or sulfates in groundwater). In general, the development of MRD can be attributed to either physical and/or chemical mechanisms, although the two often act together to initiate and propagate distress. The principle recognized mechanisms are summarized in Table 1.

MRD will generally manifest itself on the pavement surface as fine cracking or as material degradation, such as scaling or spalling. The distress may be isolated in the vicinity of joints or cracks or distributed over the pavement surface. Discoloration of the concrete, sometimes referred to as staining, is also a common feature, as is the observation of exudates in cracks. In some instances, large-scale concrete expansion may occur, resulting in blowups at joints and displacement of fixed structures. Depending upon the type of distress and the environment to which the pavement is exposed, these distresses may occur as soon as a few years following construction. In other cases, noticeable pavement deterioration will not be observed until much later in the pavement's service life.

Table 1: Summary of key materials-related distresses in concrete pavements.

Type of MRD	Surface Distress Manifestations and Locations	Causes/ Mechanisms	Time of Appearance	Prevention or Reduction
<i>MRD Due to Physical Mechanisms</i>				
Freeze-Thaw Deterioration of Hardened Cement Paste	Scaling, spalling or map-cracking, generally initiating near joints or cracks; possible internal disruption of concrete matrix.	Deterioration of saturated cement paste due to repeated freeze-thaw cycles.	1–5 years	Addition of air-entraining agent to establish protective air-void system.
Deicer Scaling/Deterioration	Scaling or crazing of the slab surface with possible alteration of the concrete pore system and/or the hydrated cement paste leading to staining at joints/cracks.	Deicing chemicals can amplify freeze-thaw deterioration and may interact chemically with cement hydration products.	1–5 years	Provide minimum cement content of 335 kg/m ³ , limit water–cement ratio to no more than 0.45, and maximize the time period after curing before the application of deicer chemicals.
Freeze-Thaw Deterioration of Aggregate	Cracking parallel to joints and cracks and later spalling; may be accompanied by surface staining.	Freezing and thawing of susceptible coarse aggregates results in fracturing and/or excessive dilation of aggregate.	10–15 years	Use of non-susceptible aggregates or reduction in maximum coarse aggregate size.
<i>MRD Due to Chemical Mechanisms</i>				
Alkali–Silica Reactivity (ASR)	Map cracking over entire slab area and accompanying expansion-related distresses (joint closure, spalling, blowups).	Reactions involving hydroxyl and alkali ions in pore solution and reactive silica in aggregate resulting in the build-up of expansive pressures within aggregate, until tensile strength of surrounding paste matrix is exceeded, resulting in cracks.	5–15 years	Use of non-susceptible aggregates, addition of pozzolans to mix, limiting total alkalis in concrete, minimizing exposure to moisture, addition of lithium compounds.
Alkali–Carbonate Reactivity (ACR)	Map cracking over entire slab area and accompanying pressure-related distresses (spalling, blowups).	Expansive reaction involving hydroxyl and alkali ions in pore solution and certain dolomitic aggregates resulting in dedolomitization and brucite formation.	5–15 years	Avoid susceptible aggregates, significantly limit total alkalis in concrete, blend susceptible aggregate with quality aggregate or reduce size of reactive aggregate.
External Sulfate Attack	Fine cracking near joints and slab edges or map cracking over entire slab area, ultimately resulting in joint or surface deterioration.	Expansive formation of ettringite that occurs when external sources of sulfate (e.g., groundwater, deicing chemicals) react with the calcium sulfoaluminates.	1–5 years	Use w/c below 0.45, minimize C ₃ A and C ₄ AF content in cement, use blended cements, use pozzolans.
Internal Sulfate Attack	Fine cracking near joints and slab edges or map cracking over entire slab area.	Formation of ettringite from internal sources of sulfate that results in either expansive disruption in the paste phase or fills available air voids, reducing freeze-thaw resistance.	1–5 years	Minimize internal sources of slowly soluble sulfates, minimize tricalcium aluminate content in cement, avoid high curing temperatures.
Corrosion of Embedded Steel	Spalling, cracking, and deterioration at areas above or surrounding embedded steel.	Chloride ions penetrate concrete, resulting in corrosion of embedded steel, and formation of high-volume oxidation products and resultant expansion.	3–10 years	Reduce the permeability of the concrete, provide adequate concrete cover, protect steel, or use corrosion inhibitor.

OBJECTIVE

Over the past 20 years MRD has shortened the service life of several projects within the greater Metro Detroit area. Generally, the observed deterioration has starts with cracking and crumbling at the joints, eventually progressing over time inward over the slab. The 1992 US-23 project in Genesee County, (CS 25031-30798A) which was reconstructed in 2005, is an example of this destructive process. Recent research studies focusing on materials-related distress (MDOT Research Reports RC1443 and RC1425) have confirmed that alkali-silica reactivity, paste freeze-thaw damage, and aggregate freeze-thaw damage exist within Michigan's concrete pavements.

The original study was a multi-phase project with the following objectives:

- Identify, to the extent possible, the cause of MRD on a selected number of pavement sections to determine if previous work fully captured the range of problems.
- Design and conduct a laboratory study to investigate the observed distress(es) with the purpose of selecting mixture properties to prevent the occurrence of such distress(es) in future concrete pavement construction.
- Make recommendations for the treatment of the existing pavement sections and prevention of deterioration in future pavement construction, including recommendations for materials selection, mix design, and construction practices.

The project, as proposed, was to progress in two phases, the first of which was a review of additional literature and evaluation of field sites. Phase I was summarized in an interim report that detailed the results of the field evaluation. Based on the findings from Phase I, a research plan for a laboratory investigation of factors leading to MRD was developed for Phase II. Unforeseen factors and constraints on the overall study's allocated time forced Phase II and other subsequent work beyond Phase I to be redefined as a new project in MDOT's research program. This report documents work completed for Phase I and includes a proposed agenda for future subsequent work.

THIS PAGE INTENTIONALLY LEFT BLANK

SCOPE

A total of 40 core specimens were received, representing six pavements sites as summarized in Table 2. Eight of the cores were returned to MDOT for their examination. The numbers of cores analyzed from each site, and the number of cores returned are listed in Table 3. In the case of the I-696 site, no intact cores were left, so only core fragments could be returned. Data collected from the cores are included in Appendices A through F, and organized according to core site.

Table 2: Summary of coring sites.

Route	CS/Project No.	Location	Sub-location	Year Constr.	Pavement type	Coarse aggr. type	MRD Severity Level	Visual Description of MRD pavement distress
I-696	50062/00703A	WB, I-94 interchange	-	1978	10 in. thickness 71' JRCPC slabs	Blast furnace slag	None	None visible
	50062/ 36001A		Median Lane Outside Lane	1995	11 in. thickness 27' JRCPC slabs		Low High	Joint Staining Severe transverse and longitudinal joint spalling w/cold patching
M-5	63192/ 34962A	SB, 12 Mile Rd. to 14 Mile Rd.	Outside Lane	1998	10 in. thickness 41' JRCPC slabs	Blast furnace slag	Low/Moderate	Low/moderate transverse and longitudinal joint spalling w/staining.
			Median Lane				None	None visible
M-59	50022/ 05675A	EB, Elizabeth Lake Rd. to Romeo Plank Rd.	Outside Lane	1997, 1998	10 in. thickness 27' JRCPC slabs.	Blast furnace slag	Moderate	Mid-slab delamination w/ surface drying shrinkage cracks.
			Middle Lane				High	Longitudinal joint deterioration w/cold patch
			Shoulder				Low	Surface drying shrinkage cracks
M-14	81105/ 38009A	EB, I-94 to Huron River	Outside Lane	2000	11 in. thickness JPCP	Carbonate (Rockwood)	Low/Moderate	Longitudinal joint spalling w/pronounced staining.
US-23	58034/ 32750A	NB, SHRP Sec. 19	Outside Lane	1993	11 in. thickness JPCP	Carbonate (Silica)	High	Severe transverse and longitudinal joint spalling w/cold patching
US-23	58034/ 32750A	SB, MDOT Aggregate Test Road, Sec. B	Outside Lane	1992	10 in. thickness 27' JRCPC slabs.	Blast furnace slag	None	Mid-panel transverse cracking w/spalling

Table 3: List of cores.

Core Site	Description	# of cores received	# of cores returned
WB I-696	1978	4	0
	1995 Median lane	4	0
	1995 Outside lane	5	0
SB M-5	Outside lane	4	2
	Median lane	4	2
EB M-59	Outside lane	4	2
	Middle lane	1	0
	Shoulder	2	0
EB M-14	Outside lane	5	2
NB US-23	SHRP Sec. 19	4	0
SB US-23	MDOT Aggr. Test Road, Sec. B	2	0

THIS PAGE INTENTIONALLY LEFT BLANK

METHODOLOGY

Upon receipt, cores were photographed and individual cores selected from each site for further analysis. At a minimum, one core near the joint, and one core away from the joint were selected from each site to represent various conditions present as visible at the pavement surface. Whenever possible, core locations were selected according to FHWA-RD-01-164 Guidelines for Detection, Analysis, and Treatment of Materials-Related Distress in Concrete Pavements - Volume 2: Guidelines Description and Use, which recommends two cores from the joint, and two to three additional cores to represent the rest of the panel. One core from the joint should be located between dowel bars, and the other core from the joint should be located over a dowel bar. For the non-joint cores, one core should be taken near the panel corner, and another core should be taken mid-panel in an area showing minimal to no deterioration. In slabs with MRD distributed throughout the slab, another core should be taken mid-panel in an area showing deterioration. The selected cores were stabilized with epoxy, if necessary, and cut in half: one half representing the top half of the core and the other half representing the bottom half of the core. Each half was then cut into slabs to obtain rectangular cross-sections for the full depth of the pavement from top to bottom. One slab from each half was polished, scanned, (with a flatbed scanner) and examined according to ASTM C457 *Standard Test Method for Microscopical Determination of Parameters of the Air-Void System in Hardened Concrete* to determine the air-void parameters. Next, the polished slabs were either treated with sodium cobaltinitrite, a stain that turns potassium-rich alkali-silica reaction products yellow, or phenolphthalein, a pH indicator that turns calcium hydroxide rich cement paste pink, (leaving carbonated cement paste or calcium hydroxide depleted cement paste unaffected). After staining, the slabs were examined with a stereomicroscope and scanned. The final step was to color the polished slabs black, press white powder into the air voids and cracks. Additional unpolished slabs were retained for use in thin section preparation. Fluorescence measurements were taken from the cement paste in thin section and correlated to water-to-cement (w/c) ratio values from fluorescence measurements collected from 28-day cured mortar standards of known w/c ratio as described in Appendix G.

THIS PAGE INTENTIONALLY LEFT BLANK

DISCUSSION OF RESULTS

The equivalent w/c ratio measurements from cores from all of the sites are summarized in Table 4. The air-void parameters measured from cores from all of the sites are summarized in Table 5. For the calculation of the air-void parameters, points and lineal intercepts that fell on portions of air voids that had since been filled with secondary mineral deposits (i.e. ettringite or ASR gel) were considered as additions to the cement paste. Discussions on a site by site basis follow.

Table 4: Equivalent w/c ratio, as compared to 28-day cured mortar standards.

Core Site	Description	MTU ID	Equivalent w/c ratio	
			Avg. of 12	Std. dev.
WB I-696, I-94 interchange	1978	696-1	0.35	0.02
	1995 median lane	696-8	0.37	0.01
	1995 outside lane	696-11	0.36	0.04
SB M-5, 12 Mile Rd. to 14 Mile Rd.	Outside lane	M5-5	0.30	0.02
	Median lane	M5-2	0.35	0.05
EB M-59, Hayes Rd. to Romeo Plank Rd.	Outside lane	M59-2	0.40	0.03
EB M-14, I-94 to Huron River	Outside lane	M14-3	0.34	0.03
NB US-23, Sec. 19	Outside lane	US23-03	0.46	0.04
SB US-23, Sec. B	Outside lane	US23-07	0.33	0.03

Table 5: ASTM C 457 air-void system parameters.

Core Site	Description	MTU ID	Core location	Air content (vol.%)	Paste content (vol.%)	Aggregate content (vol.%)	Specific Surface (mm ⁻¹)	Spacing Factor (mm)
WB I-696, I-94 interchange	1978	696-5	near joint, core A	7.4	28.7	63.9	23.6	0.164
	1978	696-7	near joint, core B	6.5	26.7	66.8	22.2	0.186
	1978	696-2	away from joint, core C	6.5	28.2	65.3	19.8	0.219
	1978	696-1	away from joint, core D	9.0	27.7	63.3	15.3	0.202
	1995, median lane	696-6	near joint, core A	5.2	30.3	64.5	27.5	0.180
	1995, median lane	696-8	near joint, core B	6.3	30.6	63.1	26.9	0.170
	1995, median lane	696-4	away from joint, core C	6.0	33.4	60.6	17.8	0.274
	1995, median lane	696-3	away from joint, core D	4.2	31.1	64.7	24.3	0.229
	1995, outside lane	696-9	at joint, core A	3.7	34.7	61.3	27.5	0.223
	1995, outside lane	696-11	away from joint, core C	5.3	34.1	60.5	29.8	0.174
	1995, outside lane	696-12	away from joint, core D	5.9	32.5	61.6	35.3	0.138
SB M-5, 12 Mile Rd. to 14 Mile Rd.	Outside lane	M5-5	near joint, core B	7.3	26.9	65.7	23.9	0.154
	Outside lane	M5-8	away from joint, core D	7.3	27.8	64.9	25.2	0.152
	Median lane	M5-6	near joint, core B	8.7	25.4	65.9	22.0	0.133
	Median lane	M5-2	away from joint, core D	6.9	26.1	67.0	28.4	0.132
EB M-59, Hayes to Romeo Plank Rd.	Outside lane	M59-1	at joint, core A	6.6	28.5	64.9	23.4	0.185
	Outside lane	M59-2	away from joint, core C	9.2	27.9	62.8	16.3	0.186
	Shoulder	M59-4	at joint?, core B	8.8	27.6	63.5	16.2	0.195
	Shoulder	M59-5	at joint, core A	8.4	30.5	61.1	21.8	0.167
EB M-14, I-94 to Huron River	Outside lane	M14-2	at joint, core B	6.9	29.3	63.8	16.1	0.263
	Outside lane	M14-3	away from joint, core C	6.5	29.9	63.5	20.2	0.221
NB US-23, SHRP Sec. 19	Outside lane	US23-03	“6 ft. from edge”	6.5	28.7	64.8	18.3	0.239
	Outside lane	US23-05	at joint, core A	6.1	25.9	68.0	15.4	0.276
SB US-23, Sec. B	Outside lane	US23-07	longitudinal joint	8.9	30.4	60.6	23.1	0.147

Core Sites

WB I-696, I-94 Interchange, Roseville

This site was divided into two separate sections: one from pavement constructed in 1978 and another from a pavement constructed in 1995. The 1995 section was further divided into the median lane, which showed little sign of visible distress (Figures 1 & 2) and the outside lane which showed signs of visible distress (Figures 3 & 4).

The cores from the 1978 project were in good condition, but the transverse joint reservoir was wider than normal and filled with road debris. The cores from both 1995 sections exhibited visible crack planes at depth oriented parallel to the pavement surface, especially in the top halves of the cores. The air-void parameters are summarized in Table 5, and measured equivalent w/c ratio values are summarized in Table 4. The cores from the 1978 and the 1995 – median lane concrete had borderline air-void parameters in terms of freeze-thaw protection. Two out of the three cores analyzed from the 1995 outside lane had overall air-void parameters considered adequate for freeze-thaw protection. However, three of the cores from the outside showed a pronounced difference in the spatial distribution of air voids, with most of the entrained air concentrated in the top third of the core. Figures 5, 6, and 7 show polished slabs from the cores after treatment to enhance the appearance of air voids and cracks, illustrating the variation in the entrained air with depth. Figure 8 shows a transition zone between adequate entrained air and inadequate air in thin section from one of the cores.

The primary distinction between the 1978 site and both of the 1995 sites was the degree of alkali silica reaction products associated with fine aggregate particles. Both pavements contained similar fine aggregate, but the reactive particles from the 1995 pavement exhibited abundant reaction products and crack networks, while the reactive particles from the 1978 pavement did not. The contrast in severity of the alkali-silica reaction was observable in the images from the scanned slabs after sodium cobaltinitrite staining, as shown in Figure 9. Figures 10 and 11 show example stereomicroscope images of reactive fine aggregate particles from the 1995 median lane pavement. Figures 12 and 13 show polished slabs from the 1995 median lane pavement after treatment to enhance the appearance of cracks and voids. Figure 14 shows a deleterious chert particle in thin section.



Figure 1: Photo of I-696 median lane, with no visible distress at pavement surface.



Figure 2: Photo of I-696 median lane, with no visible distress at pavement surface.



Figure 3: Photo of I-696 outside lane, with cracks visible at pavement surface.



Figure 4: Photo of I-696, outside lane, deterioration at joints mostly covered by cold-patch material.

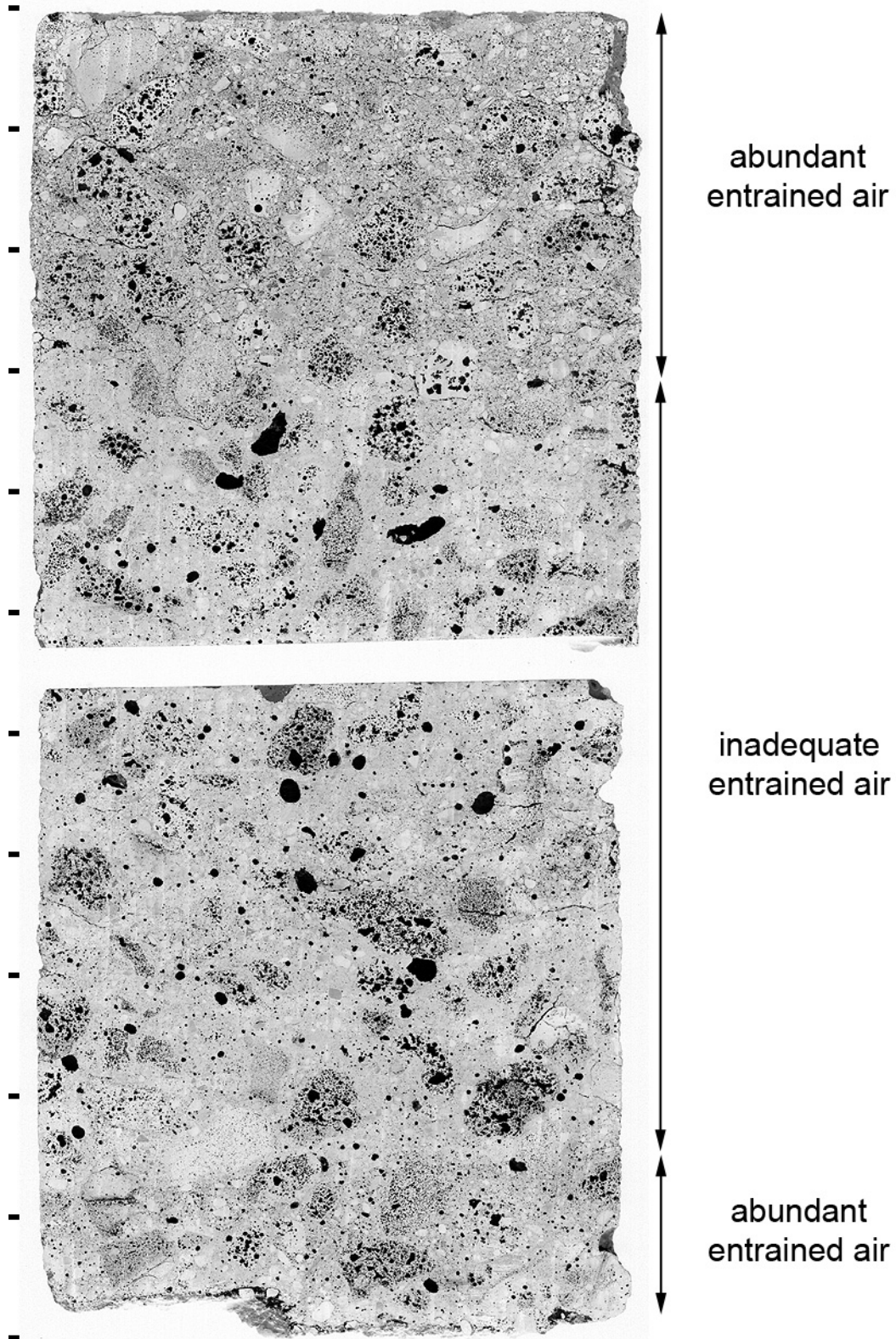


Figure 5: Slabs to represent cross section through core C, mid-panel, MTU ID 696-11, outside lane, WB I-696, after treatment to enhance air voids and cracks, tic marks every inch.

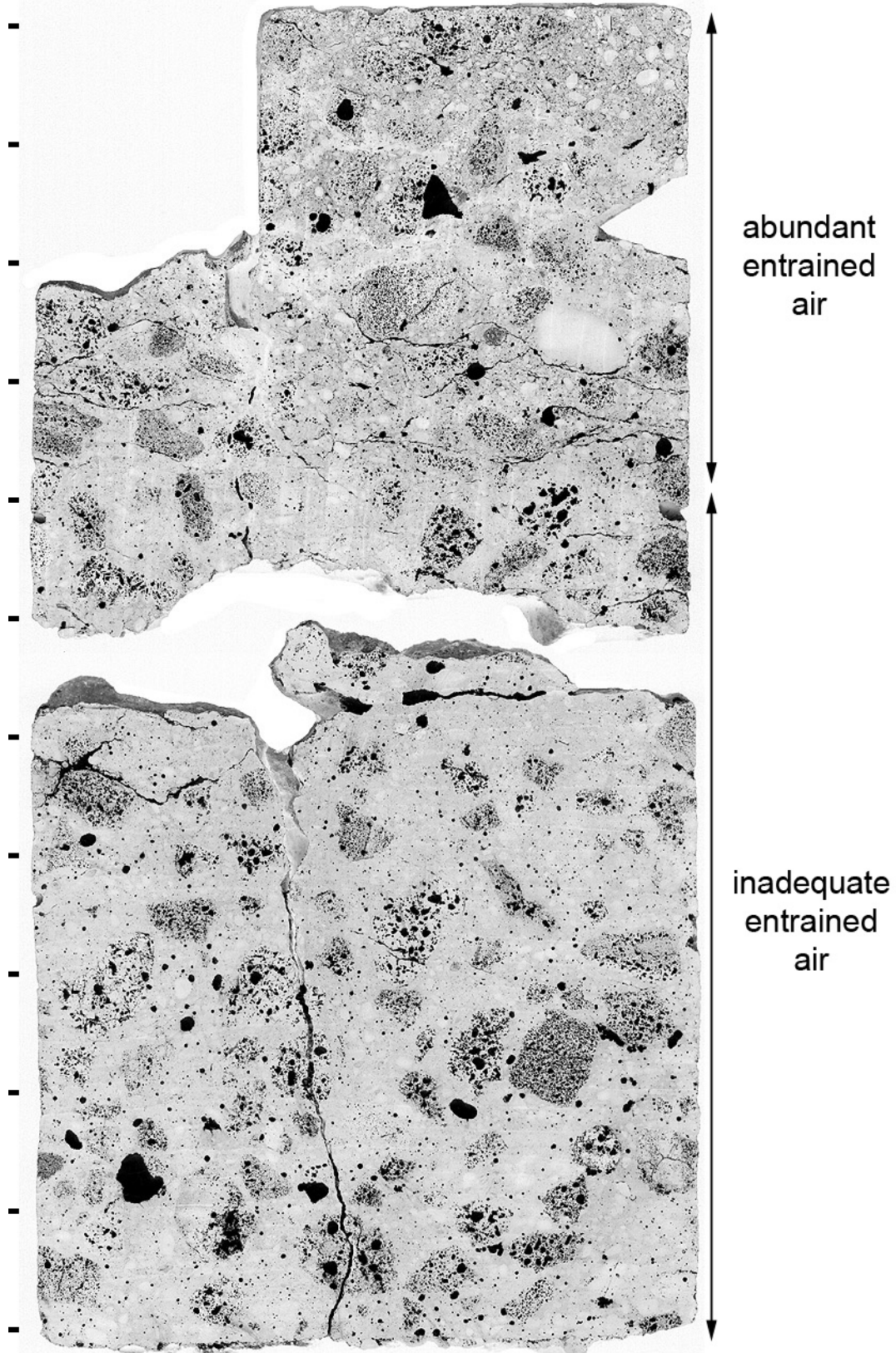


Figure 6: Slabs to represent cross section through core B, at joint, MTU ID 696-10, outside lane, WB I-696, after treatment to enhance air voids and cracks, tic marks every inch.

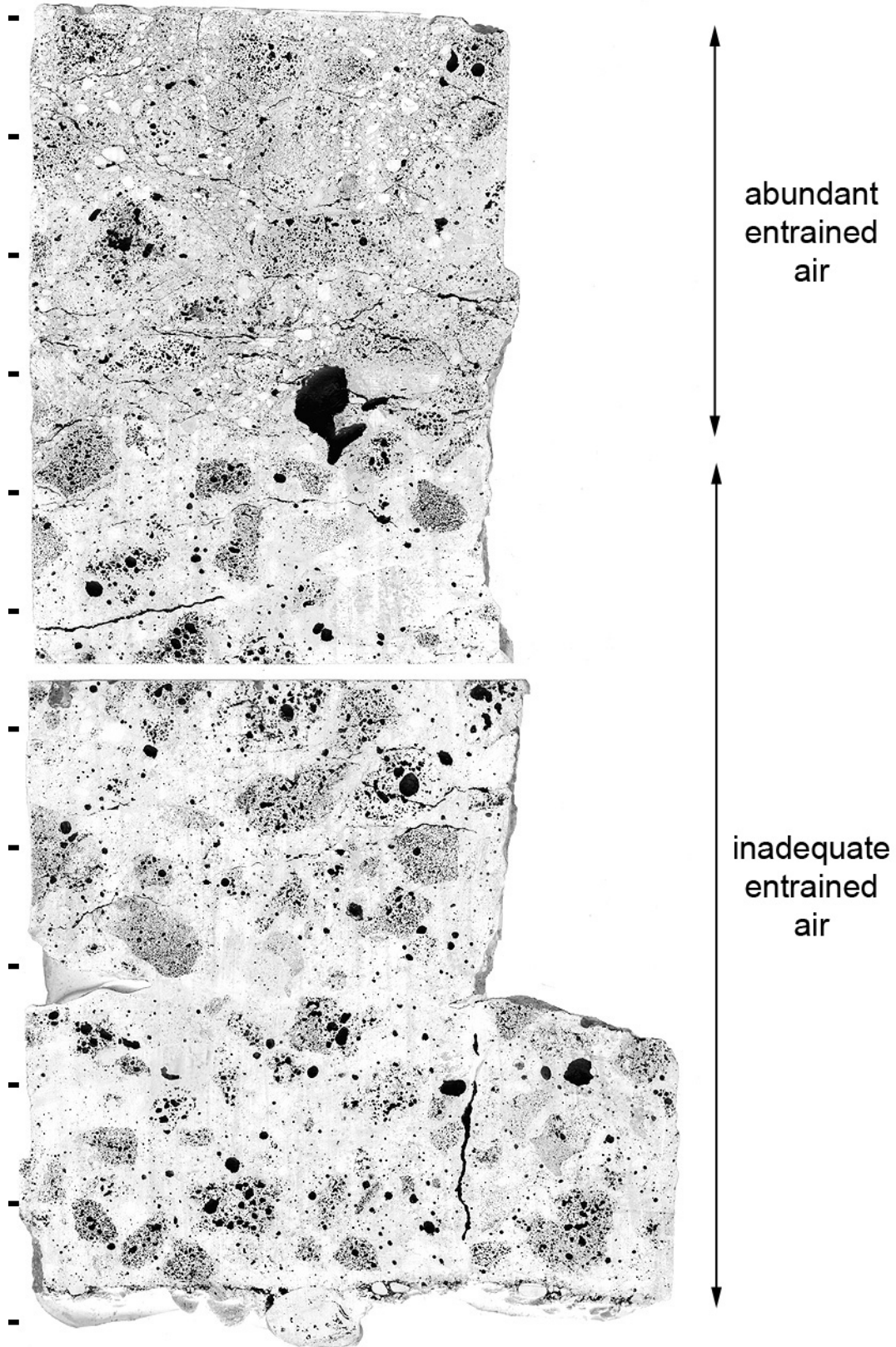


Figure 7: Slabs to represent cross section through core A, at joint, MTU ID 696-09, outside lane, WB I-696, after treatment to enhance air voids and cracks, tic marks every inch.

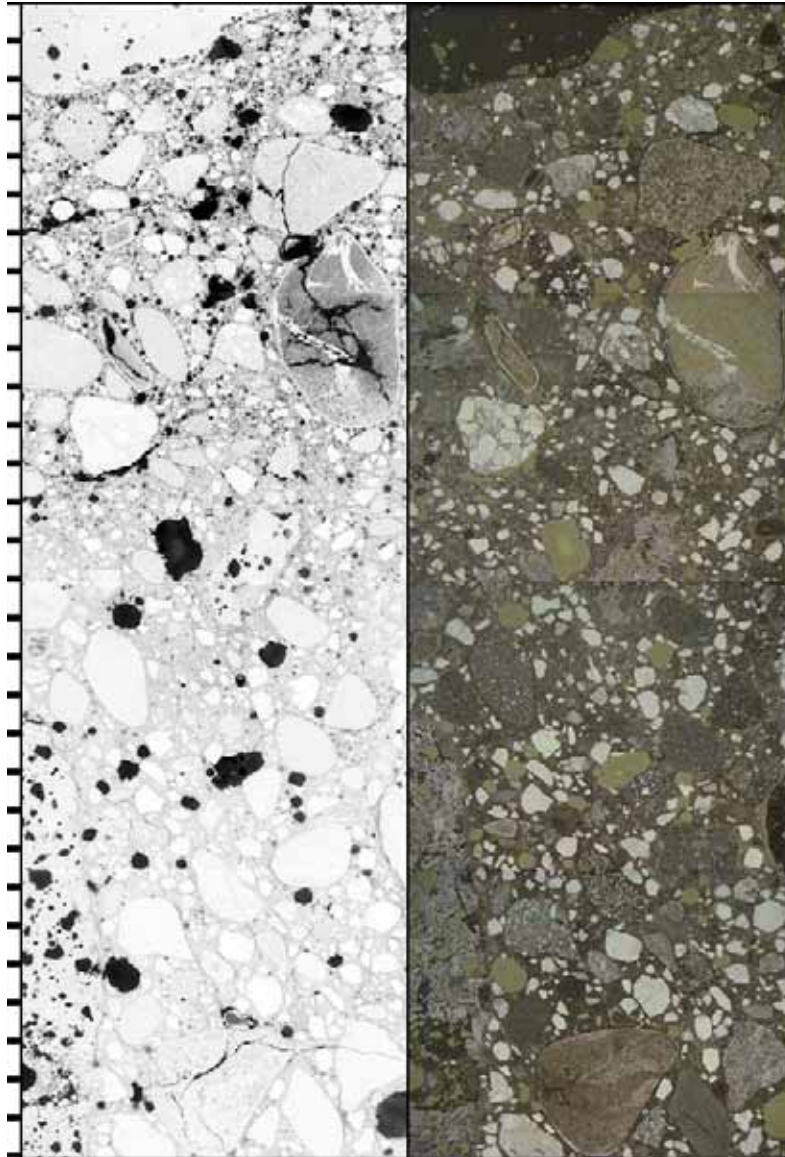
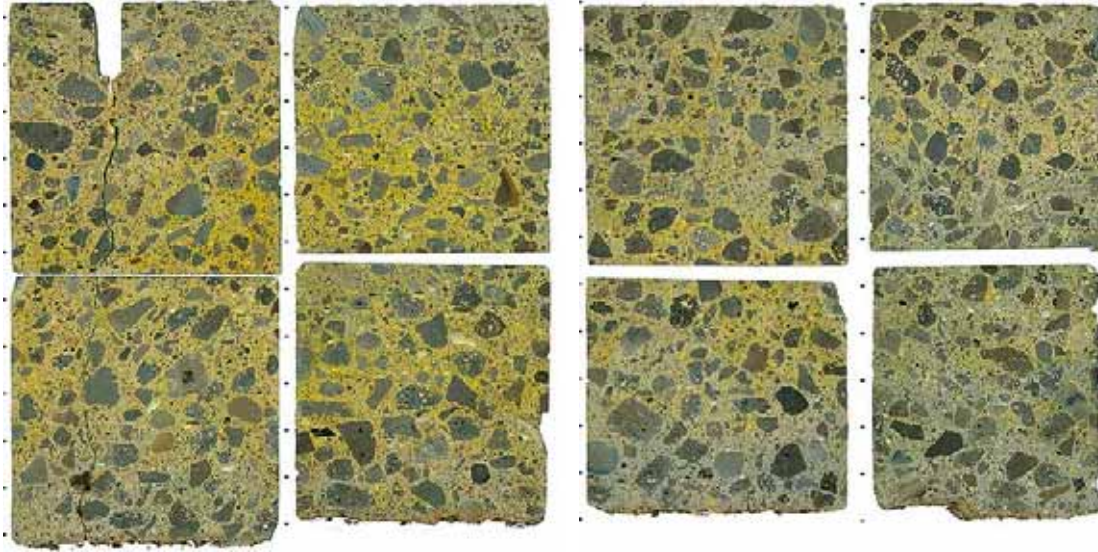
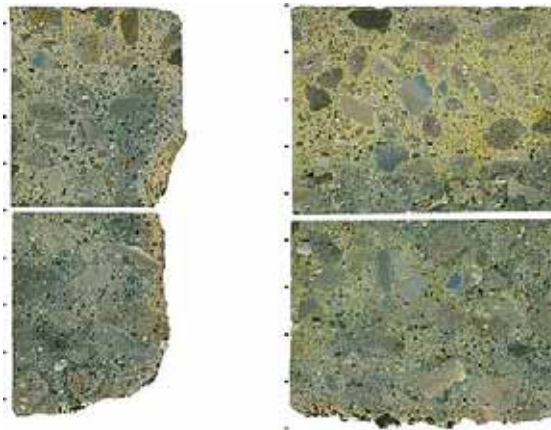


Figure 8: Epifluorescent mode (left) and transmitted light (right) images at transition between zone of abundant entrained air and zone without entrained air at a depth of approximately 3 inches (75 mm). Example from thin section prepared from core taken from I-696, outside lane, away from joint, MTU ID 696-03.



WB I-696, 1995, median lane

WB I-696, 1995, outside lane



WB I-696, 1978

Figure 9: Overview of sodium cobaltinitrite stained slabs from I-696 sites. The slabs represent full cross-sections through the pavement, with tic marks along the left hand side at one inch intervals.

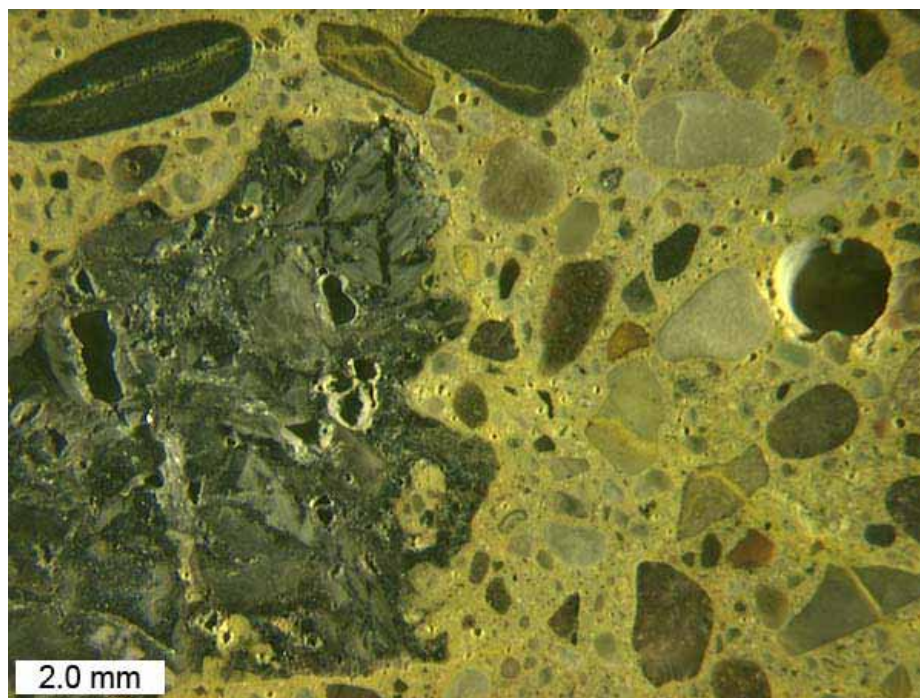
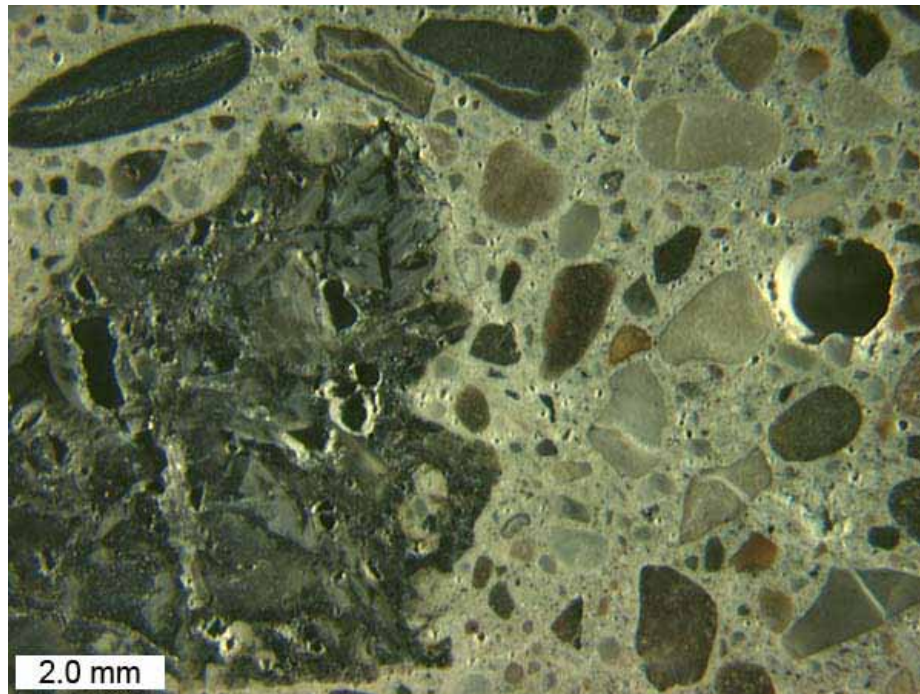


Figure 10: Alkali silica reaction in fine aggregate and associated cracking, before and after sodium cobaltinitrite stain, polished slab from I-696, constructed in 1995, median lane, away from transverse joint, top half of core D, MTU ID 696-03.



Figure 11: Alkali silica reaction in fine aggregate and associated cracking, before and after sodium cobaltinitrite stain, polished slab from I-696, constructed in 1995, median lane, away from transverse joint, top half of core D, MTU ID 696-03.

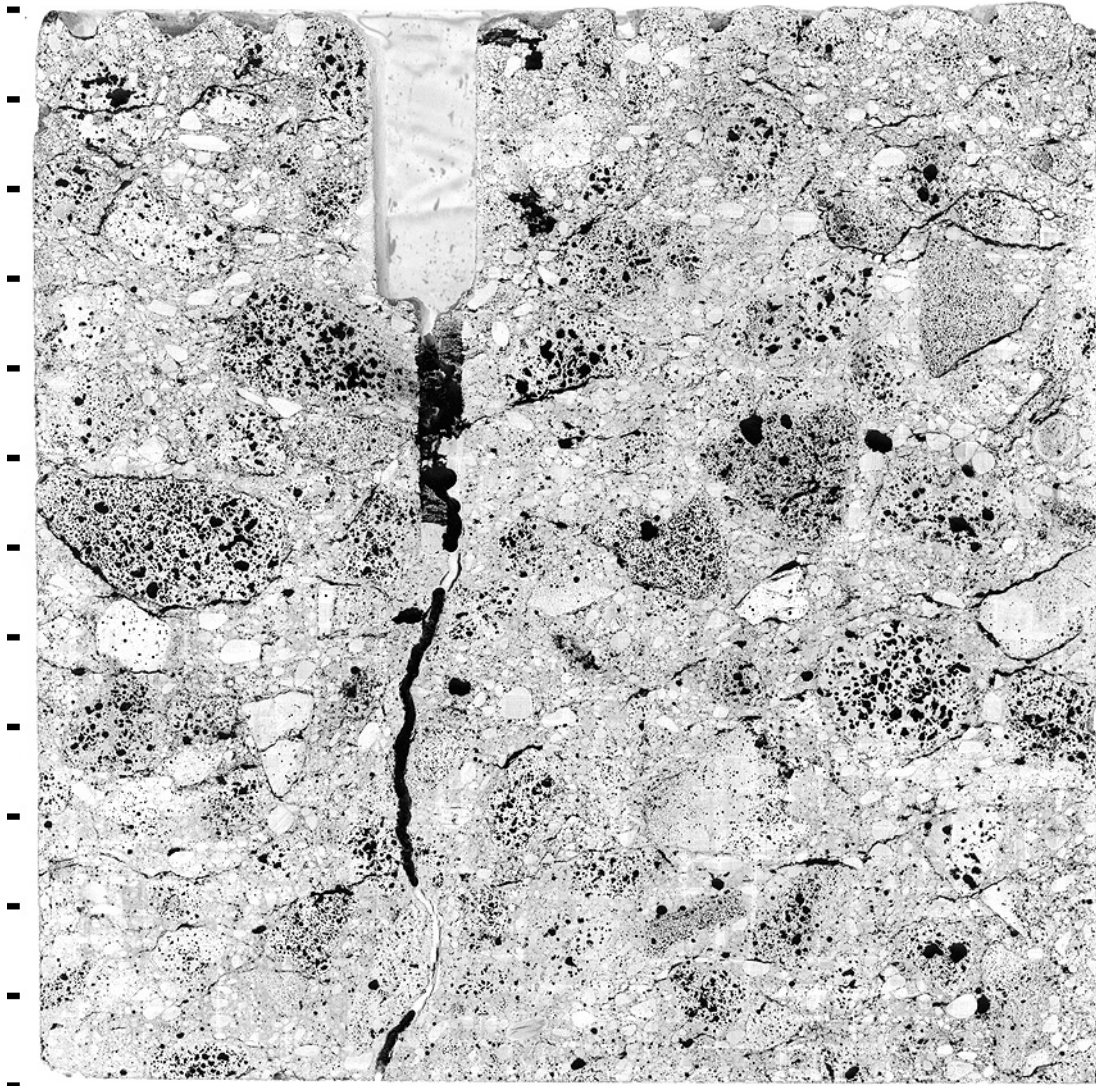


Figure 12: Slab representing cross section through top half of pavement, after treatment to enhance air voids and cracks, WB I-696, constructed in 1995, median lane, at transverse joint, core A, MTU ID 696-06, tic marks every half inch.

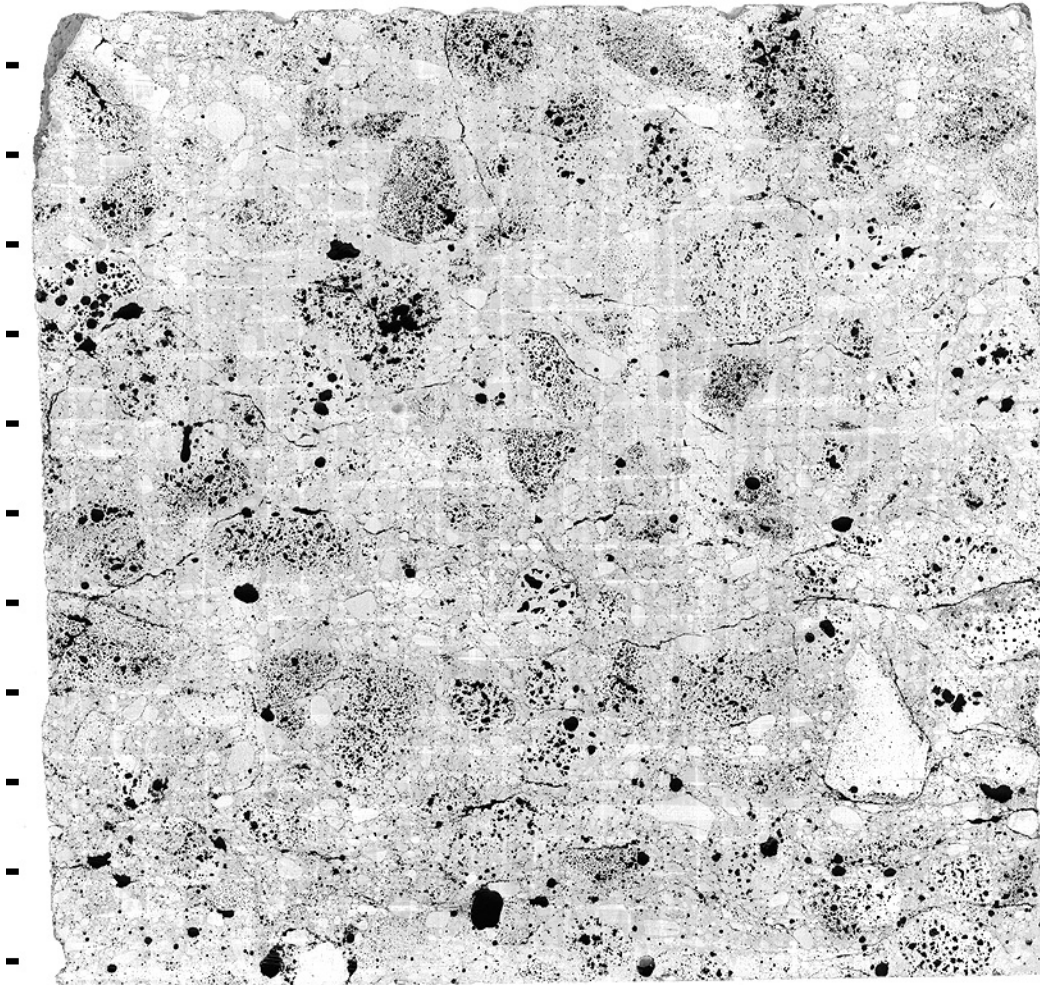


Figure 13: Slab representing cross section through top half of pavement, after treatment to enhance air voids and cracks, WB I-696, constructed in 1995, median lane, away from transverse joint, core D, MTU ID 696-03, tic marks every half inch.

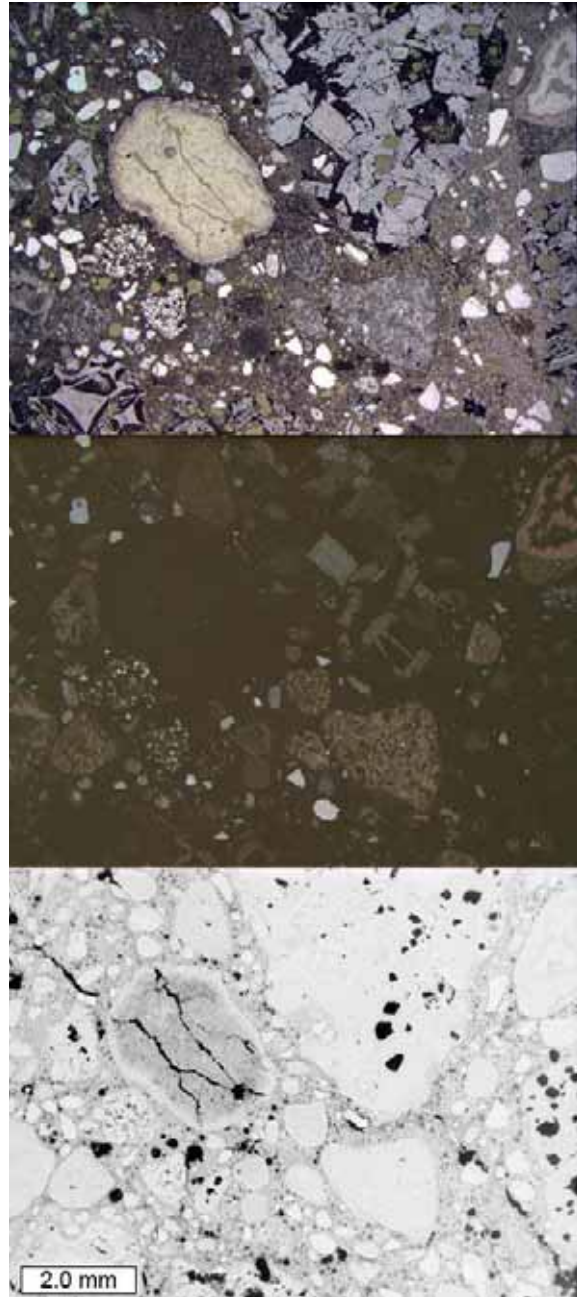


Figure 14: Example of chert particle exhibiting deleterious alkali-silica reaction in thin section prepared from core from I-696, constructed in 1995, median lane, away from transverse joint, MTU ID 696-03. From top to bottom: transmitted light, crossed-polars, and epifluorescent mode images.

THIS PAGE INTENTIONALLY LEFT BLANK

SB M-5, 12 Mile Rd. to 14 Mile Rd., Novi

This site was divided into two categories: cores from an area showing visible distress, the outside lane, and cores from an area without signs of distress, the median lane (with one exception: a single core through the longitudinal joint between the outside and median lanes). The cores from this pavement appeared to be in good condition, except for the core from the longitudinal joint, which exhibited extensive cracking oriented parallel to the joint. As a result, this core was treated differently than the others. The top 2 ½" portion of the core was trimmed, vacuum impregnated with epoxy, and cut into slabs and billets for preparation in thin section to examine the longitudinal surface cracks in cross-section. The thin sections were taken in a plane perpendicular to the longitudinal joint to show the joint in cross-section. Figure 15 shows the thin sections arranged in their original spatial context as illuminated with UV light to enhance appearance of voids and cracks filled with the fluorescent epoxy. The cracks run sub-parallel to the joint, to a depth of about 2 inches, within a zone of one half of an inch on either side of the joint. The cement paste within this zone is heavily cracked, with some increase in porosity and decrease in Ca(OH)_2 .

The other cores were slabbed, polished, stained, and examined as usual. The measured air-void parameters for both the median and outside lanes are summarized in Table 5 and were adequate for freeze-thaw protection. Results of equivalent w/c ratio measurements are included in Table 4. Figure 16 includes an overview of a polished slab after staining with sodium cobaltinitrite. Alkali-silica reactivity as observed by the staining method was limited, and only one instance of alkali-silica related cracking was observed near the pavement surface, as shown in detail in Figure 17. Figure 18 compares close-up petrographic microscope images of the cement paste in thin section from the median and outside lanes. One difference between the two sections is the concrete from median lane has fly ash, while concrete from the outside lane does not.

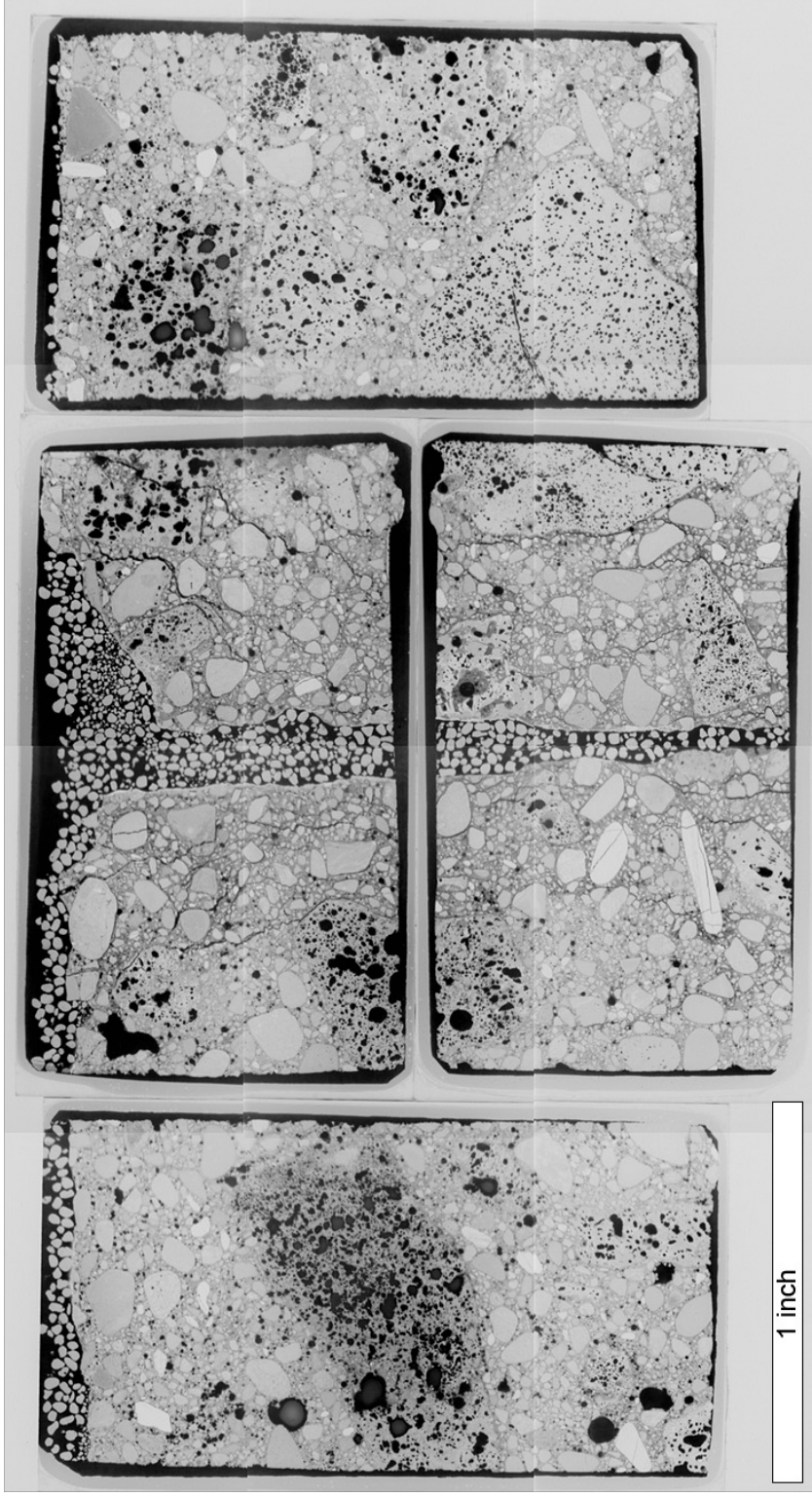
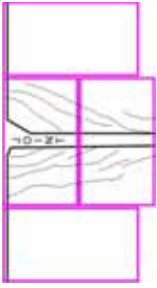


Figure 15: Thin sections arranged in their original spatial context to show the longitudinal joint in cross-section. Voids and cracks in the inverted UV fluorescent image appear dark. Coarse sand particles observed at the pavement surface and filling the joint were blended with the epoxy to conserve epoxy during impregnation of the core segment.



SB M-5, outside lane

WB M-5, median lane

EB M-59



NB US-23, Sec. 19

SB US-23, Sec. B

EB M-14

Figure 16: Overview of sodium cobaltinitrite stained slabs from all sites, excluding I-696. The slabs represent full cross-sections through the pavement, with tic marks along the left hand side at one inch intervals.

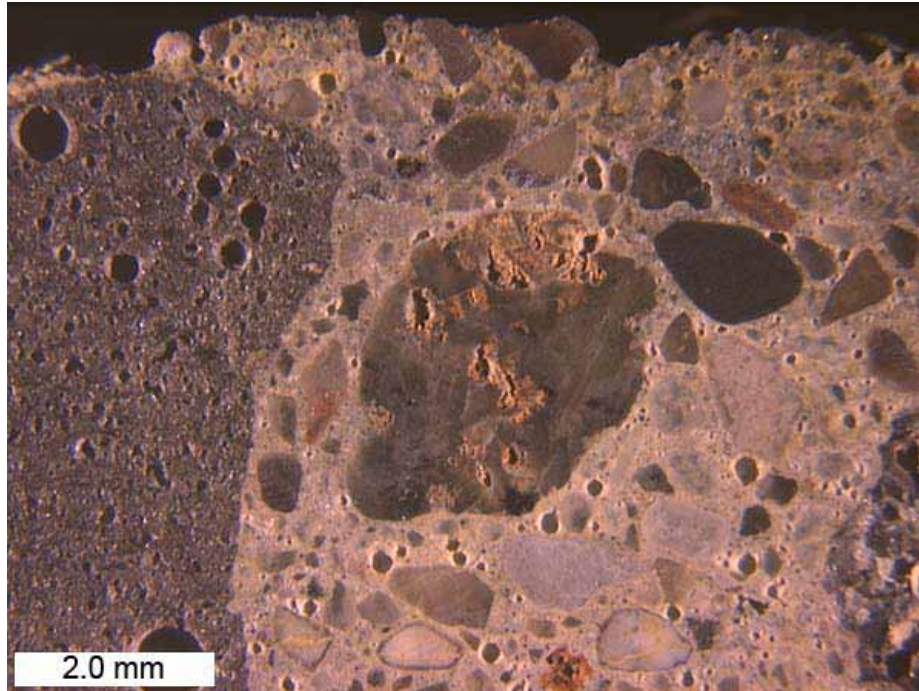


Figure 17: Successive close-up images of alkali silica reaction in fine aggregate and associated cracking near pavement surface, after sodium cobaltinitrite stain, polished slab from SB M-5, outside lane, at transverse joint, core B, MTU ID M5-05.

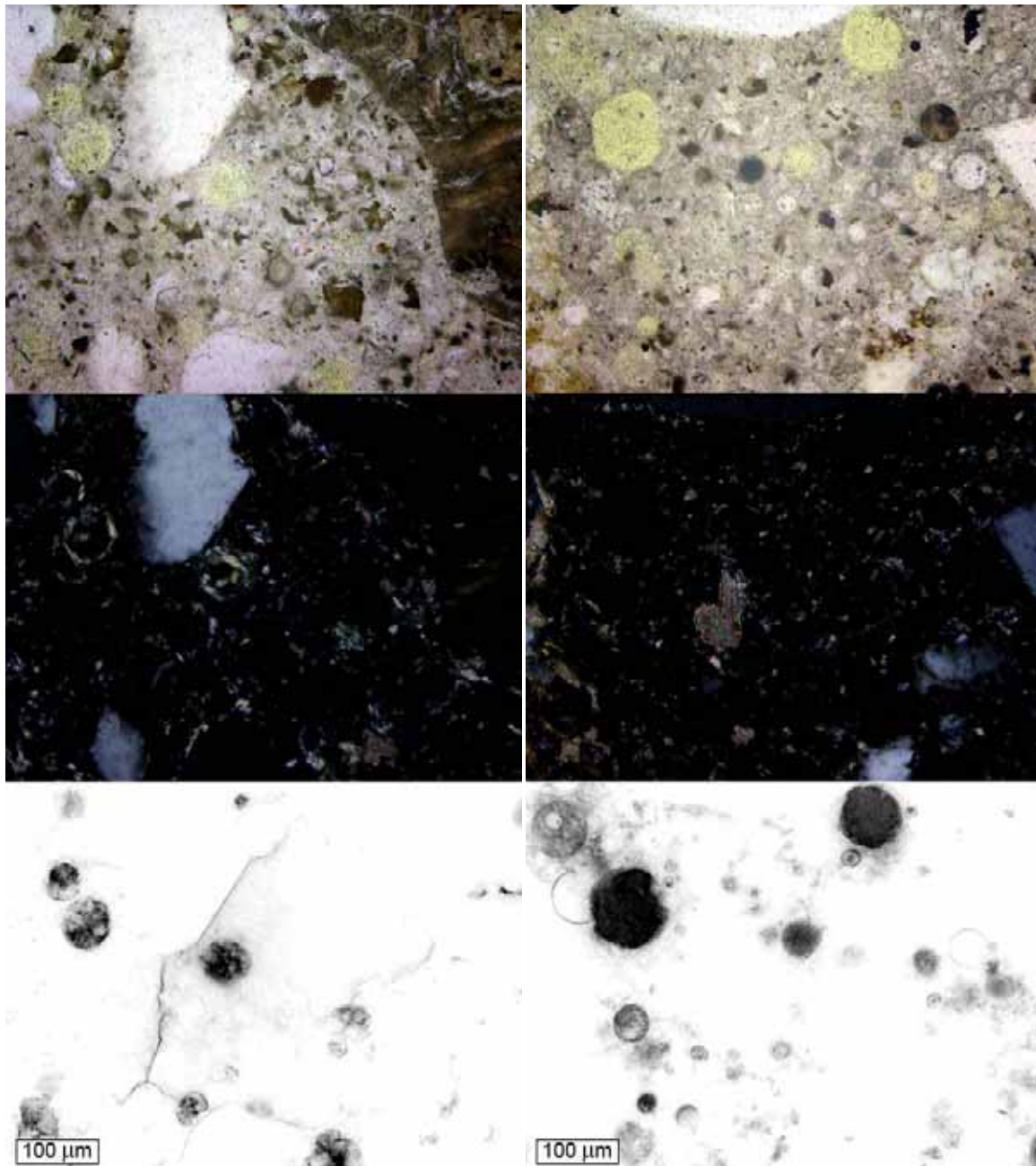


Figure 18: Examples of cement paste both without (left) and with (right) fly ash spheres. Left-hand side image from core M-5, outside lane, at transverse joint, MTU ID M5-05. Right-hand side image from core M-5, median lane, away from joint, MTU ID M5-02. From top to bottom: transmitted light, crossed-polars, and epifluorescent mode images.

THIS PAGE INTENTIONALLY LEFT BLANK

EB M-59, Hayes Rd. to Romeo Plank Rd., Clinton Township

This site consisted of four cores from the outside lane, two cores from the shoulder, and one core in very bad condition from the median lane. All of the cores exhibited cracking, especially in the top halves of the cores. The core treated with sodium cobaltinitrite picked up the stain strongly, as shown in Figure 16. Figures 19 and 20 show example stereomicroscope images of reactive fine aggregate particles from the same slab. Figure 21 shows the same polished slab after treatment to enhance the appearance of cracks and voids. Figure 22 shows a deleterious chert sand particle in thin section. The air-void parameters, summarized in Table 5, were adequate for freeze-thaw protection. Results of equivalent w/c ratio measurements are included in Table 4.

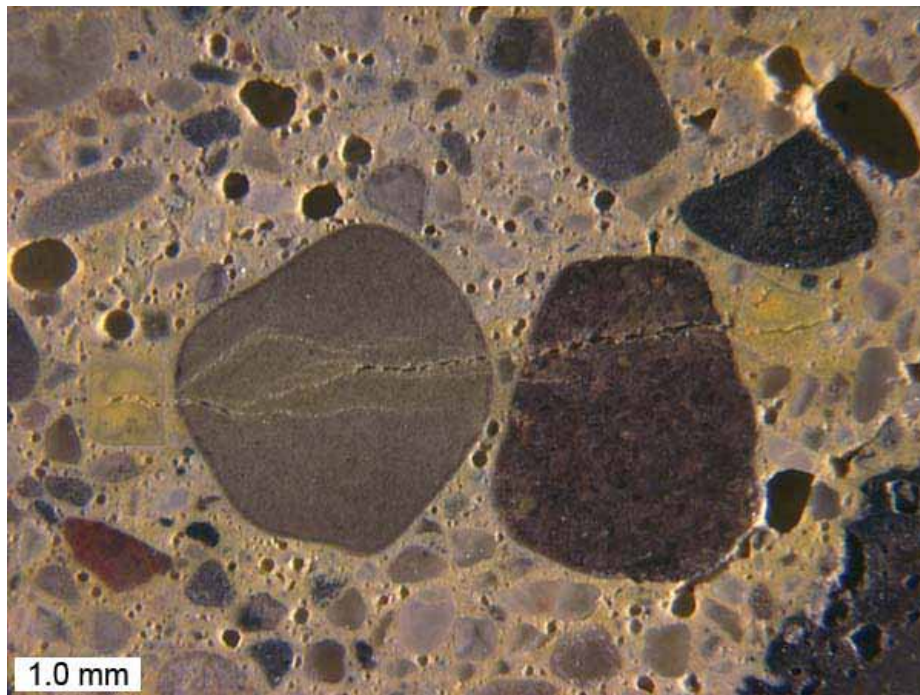
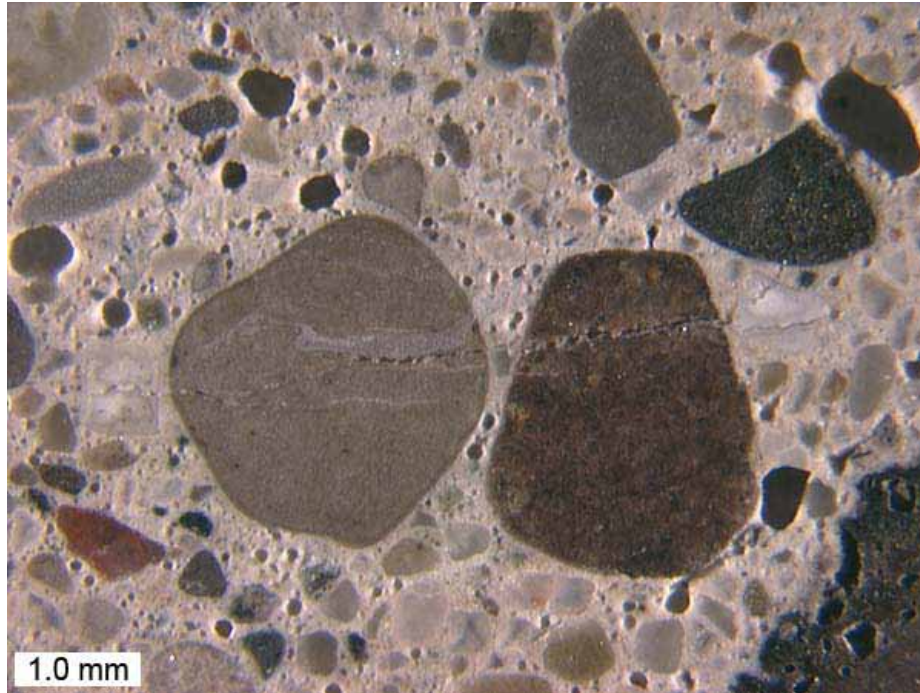


Figure 19: Alkali silica reaction in fine aggregate and associated cracking, before and after sodium cobaltinitrite stain, polished slab from top half of M-59, outside lane, away from transverse joint, core C, MTU ID M59-02.

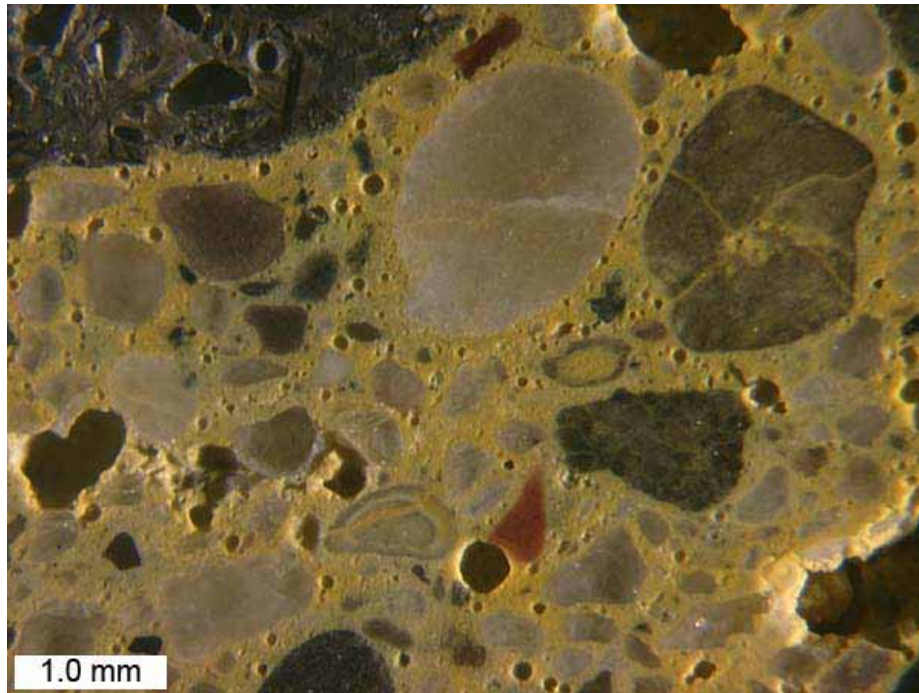
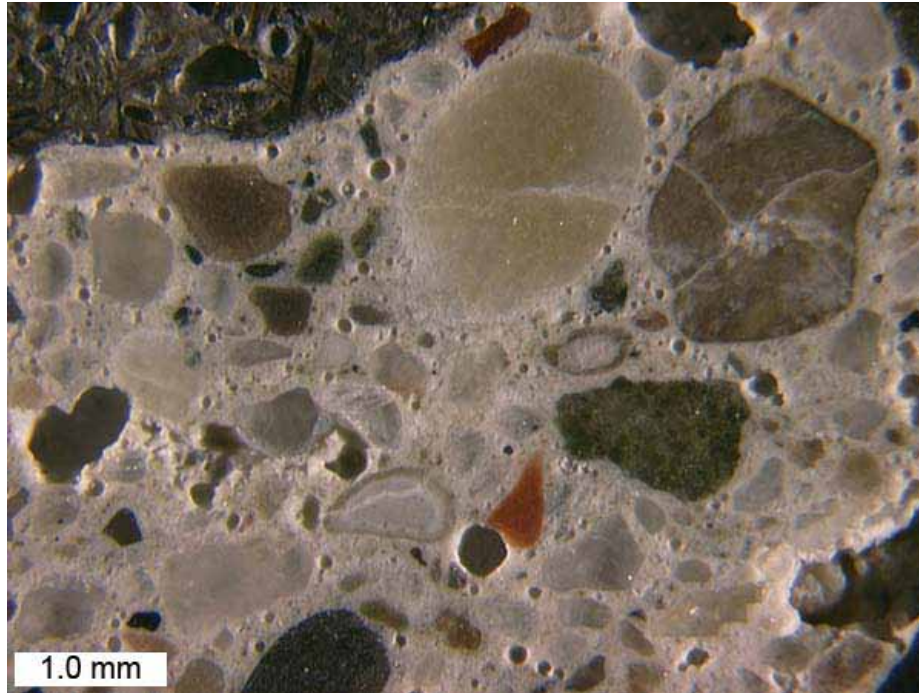


Figure 20: Alkali silica reaction in fine aggregate and associated cracking, before and after sodium cobaltinitrite stain, polished slab from top half of M-59, outside lane, away from transverse joint, core C, MTU ID M59-02.

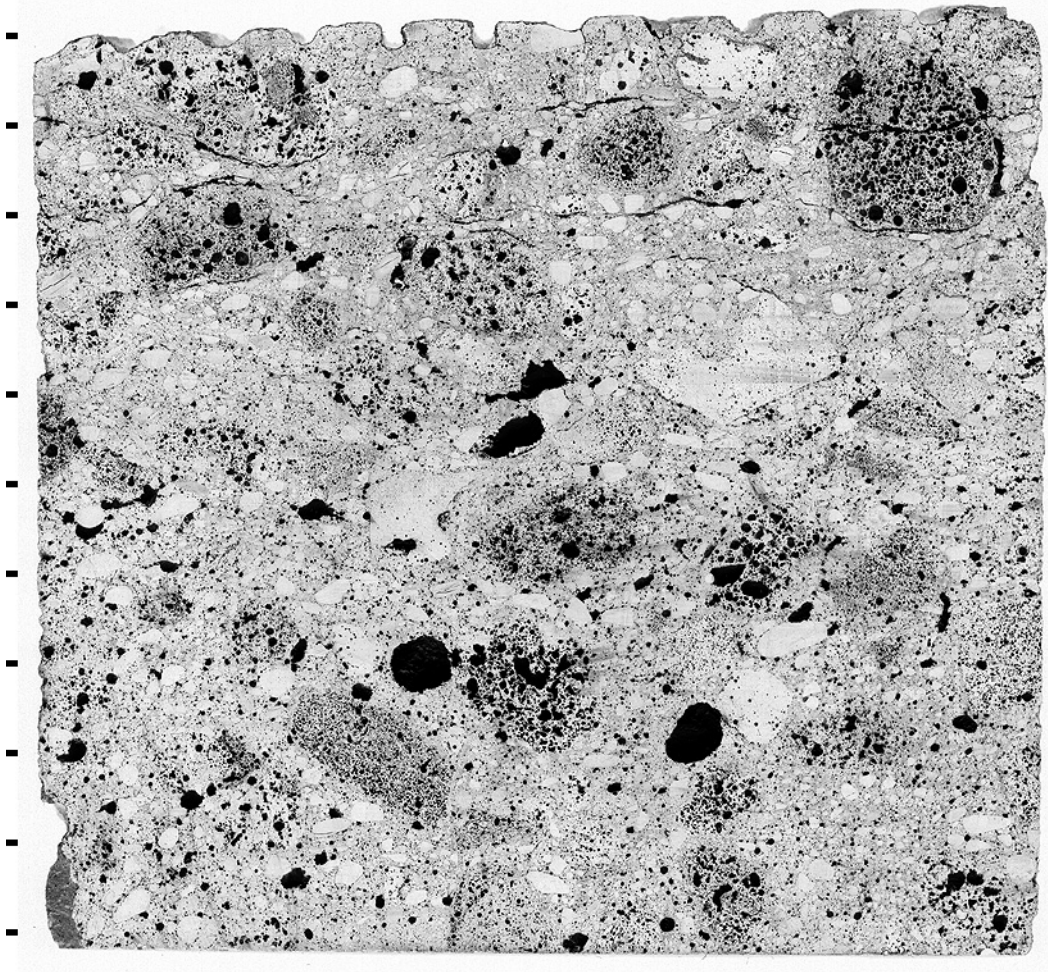


Figure 21: Slab representing cross section through top half of pavement, after treatment to enhance air voids and cracks, EB M-59, outside lane, away from transverse joint, core C, MTU ID M59-02, tic marks every half inch.

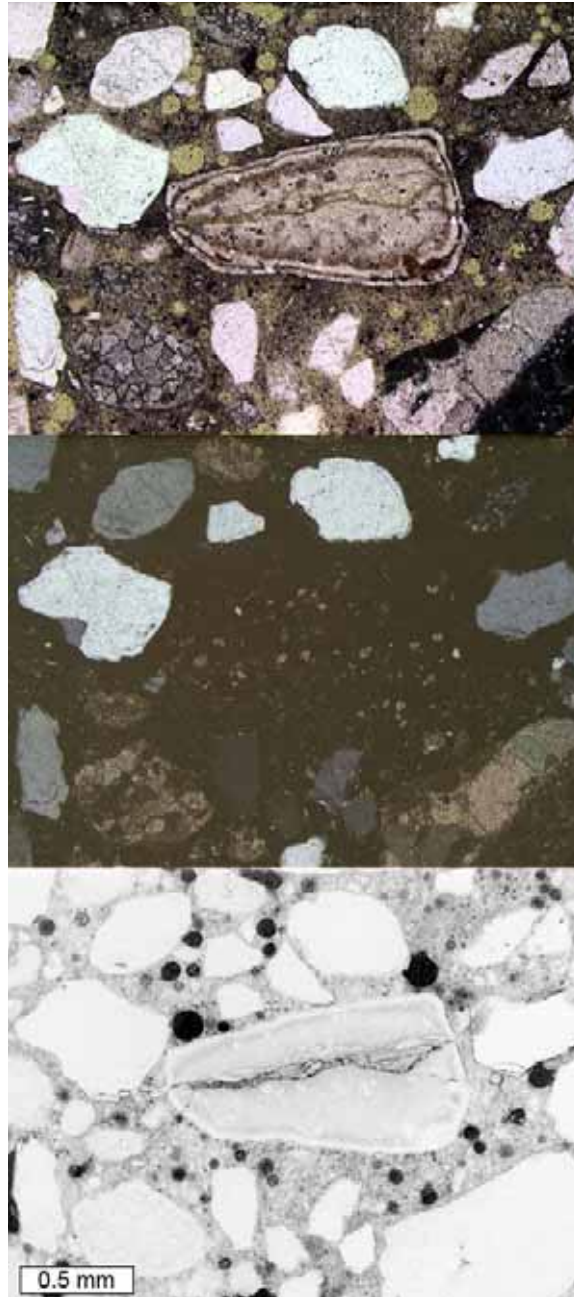


Figure 22: Example of chert particle exhibiting deleterious alkali-silica reaction, from thin section prepared from core from M-59, outside lane at joint, MTU ID M59-01. From top to bottom: transmitted light, crossed-polars, and epifluorescent mode images.

THIS PAGE INTENTIONALLY LEFT BLANK

EB M-14, I-94 to Huron River

This site consisted of five cores, three cores taken at joints, and two cores taken away from joints. All of the cores appeared to be in good condition. Slight alkali-silica reactivity was observed by the staining method, but was limited to fine aggregate particles, without any associated cracking. An overview of the slab stained with sodium cobaltinitrite is included in Figure 16. Examples of reactive particles without any associated cracking are included in Figures 23 and 24. The air-void system parameters, summarized in Table 5 were not adequate for freeze-thaw protection as the spacing factor exceeded the generally recognized upper limit of 0.200 mm. Results of equivalent w/c ratio measurements are included in Table 4. Figure 25 shows the presence of carbonate dust dispersed throughout the hardened cement paste. The source of the carbonate dust likely occurred from the crushing process to produce the coarse aggregate, as opposed to limestone dust purposefully added to or interground with the portland cement.

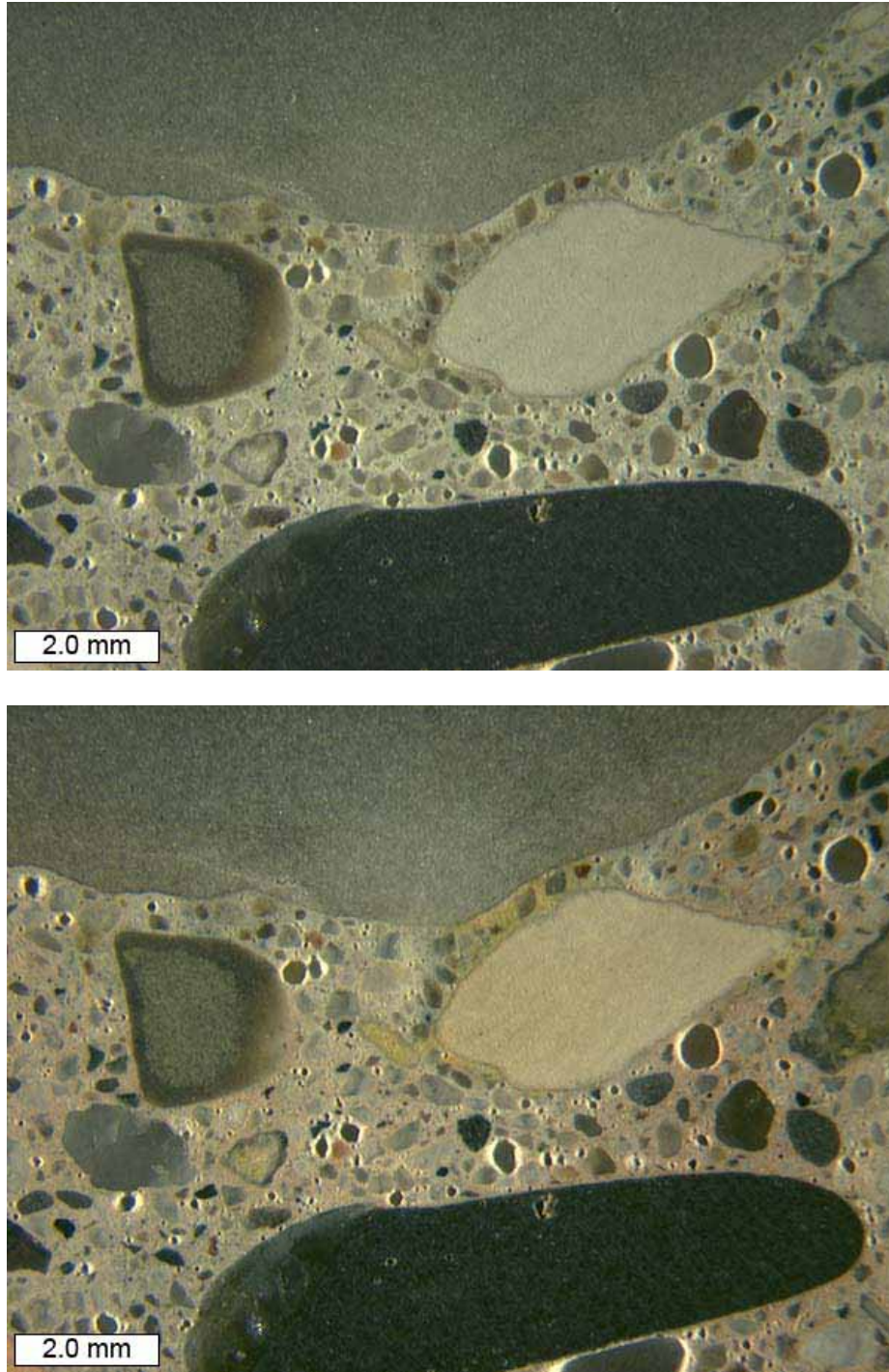


Figure 23: Alkali silica reaction in fine aggregate, with absence of cracking, before and after sodium cobaltinitrite stain, polished slab from top half of M-14, core B, at-joint, MTU ID M14-02.

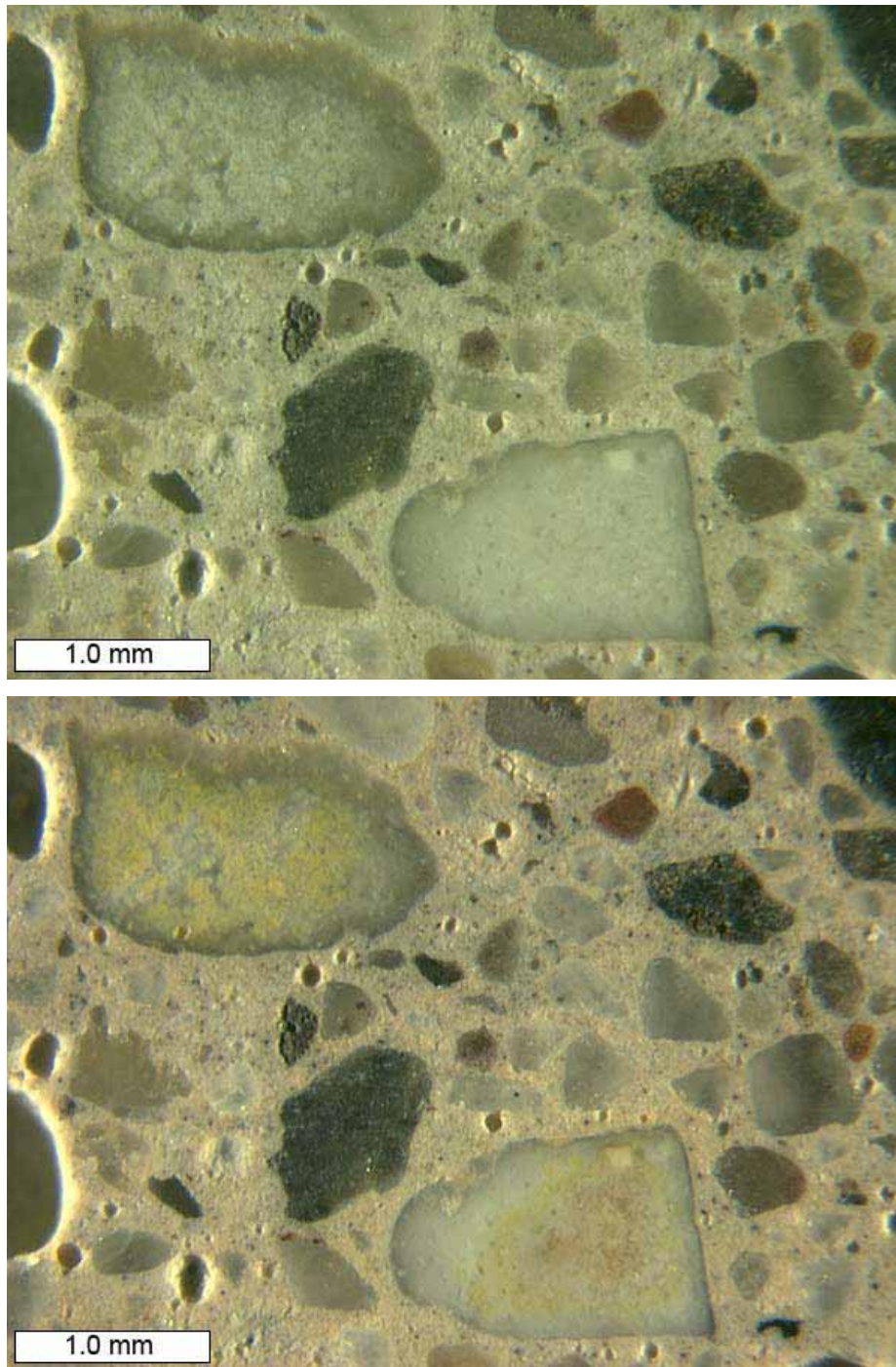


Figure 24: Alkali silica reaction in fine aggregate, with absence of cracking, before and after sodium cobaltinitrite stain, polished slab from top half of M-14, core B, at-joint, MTU ID M14-02.

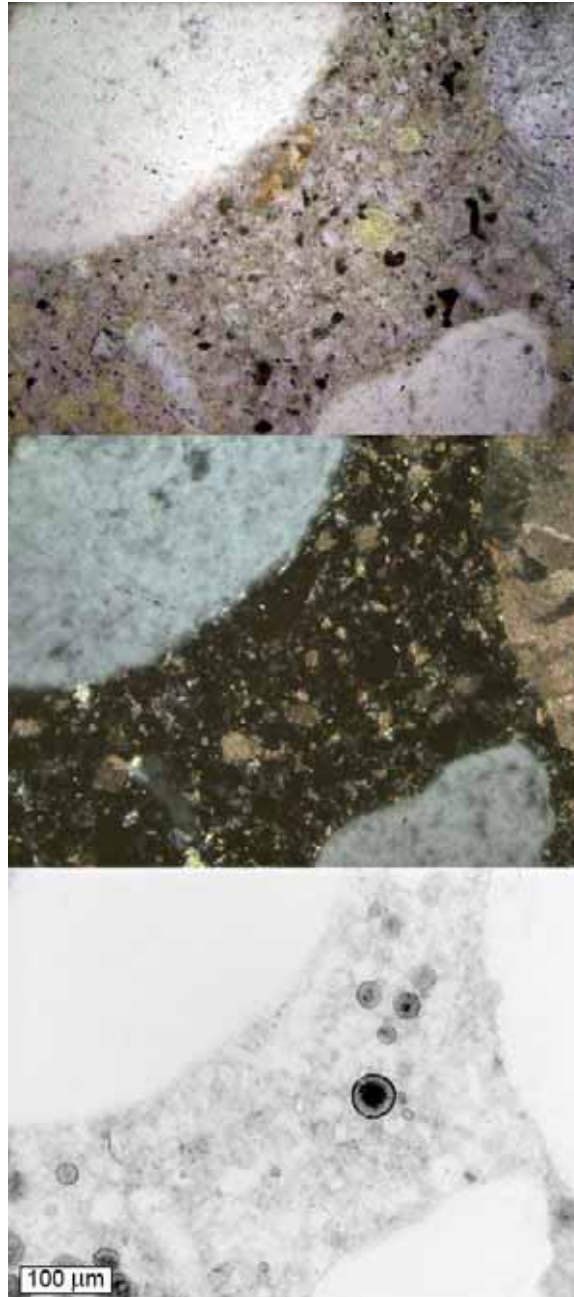


Figure 25: Carbonate dust in cement paste fraction in thin section prepared from core from M-14, away from joint, MTU ID M14-03. From top to bottom: transmitted light, crossed-polars, and epifluorescent mode images.

NB US-23, Strategic Highway Research Program (SHRP) Section 19

This site has exhibited MRD for many years and has necessitated reactive maintenance treatments. It was selected as a test site to compare its reasons for MRD initiation with newer jointed plain concrete pavement (JPCP) projects. This site consisted of four cores, one core taken at a joint, and three cores taken at increasing distances from the pavement edge. All of the cores appeared to be in good condition. Slight alkali-silica reactivity was observed by the staining method, but was limited to fine aggregate particles. Only a few of the reactive fine aggregate particles showed evidence of cracking, an example of which is shown in Figure 26. An overview of the slab stained with sodium cobaltinitrite is included in Figure 16. Figures 27 and 28 show petrographic microscope images of reactive fine aggregate particles. Figure 29 shows petrographic microscope images of carbonate dust typical of the cement paste in this concrete. The air-void parameters are summarized in Table 5. The spacing factor values from the two cores examined exceeded the recommended value for freeze-thaw protection. Results of equivalent w/c ratio measurements are included in Table 4.

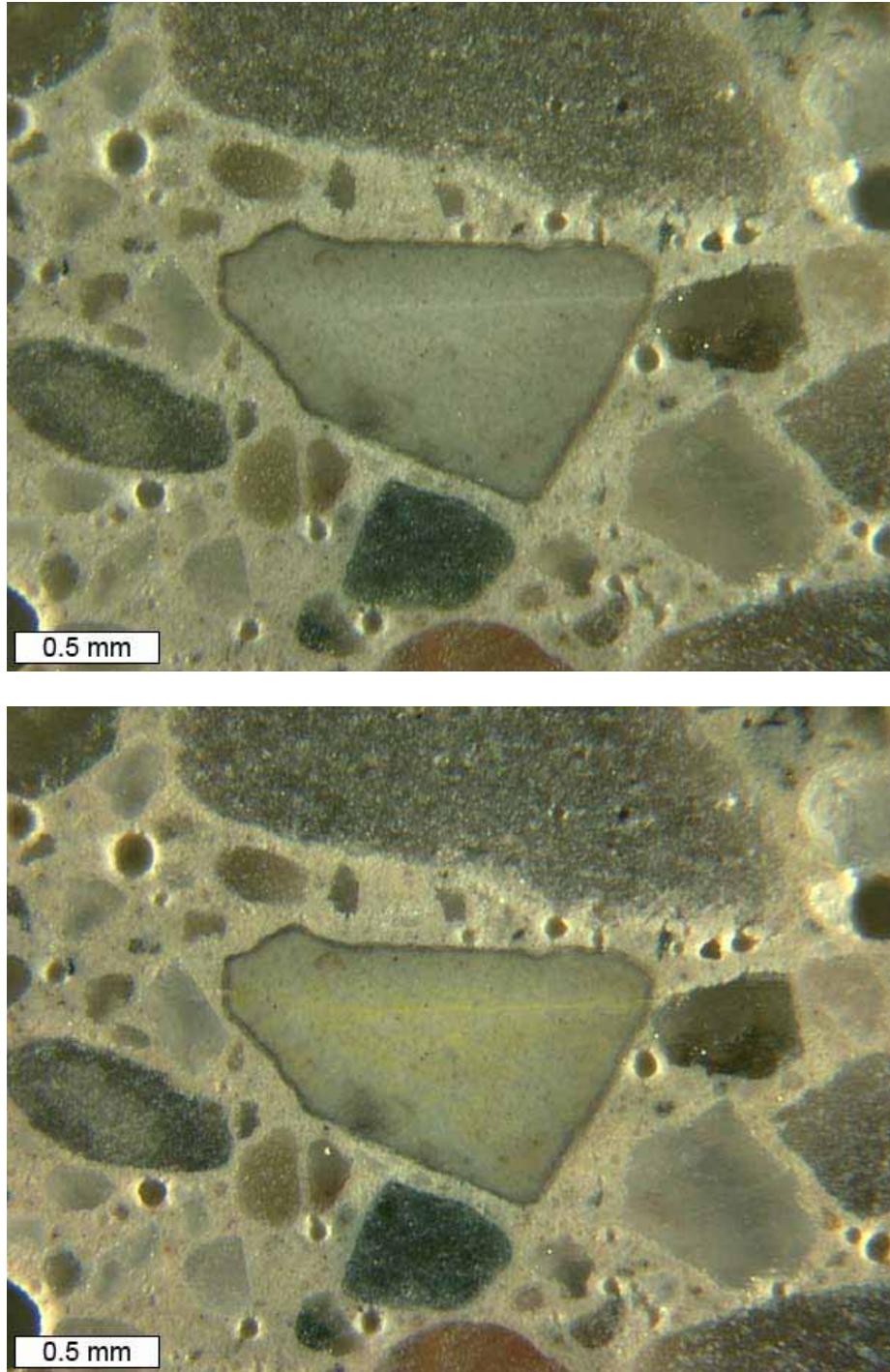


Figure 26: Alkali silica reaction in fine aggregate and associated cracking, before and after sodium cobaltinitrite stain, polished slab from top half of US-23, Section 19, at-joint, MTU ID US23-05.

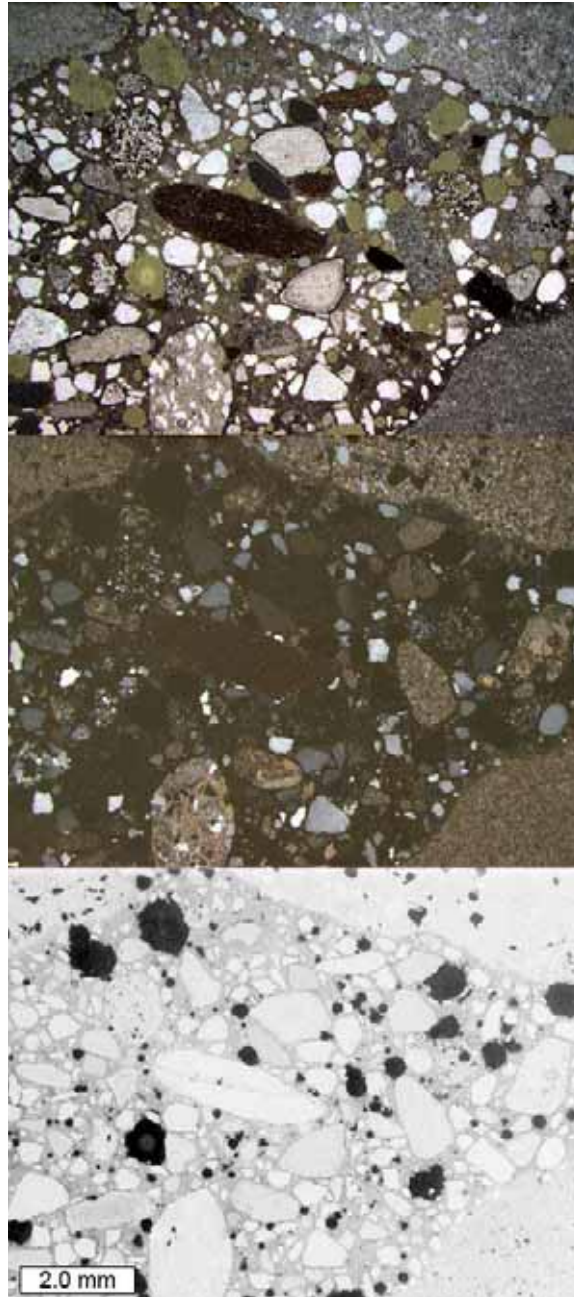


Figure 27: Example of chert particle, and brown siltstone particle, both with minor cracking associated with alkali-silica reaction, from thin section prepared from core from US23, Section 19, away from joint, MTU ID US23-03. From top to bottom: transmitted light, crossed-polars, and epifluorescent mode images.



Figure 28: Close-up example of chert particle, and brown siltstone particle from previous figure, both with minor cracking associated with alkali-silica reaction, from thin section prepared from core from US23, Section 19, away from joint, MTU ID US23-03. From top to bottom: transmitted light, crossed-polars, and epifluorescent mode images.

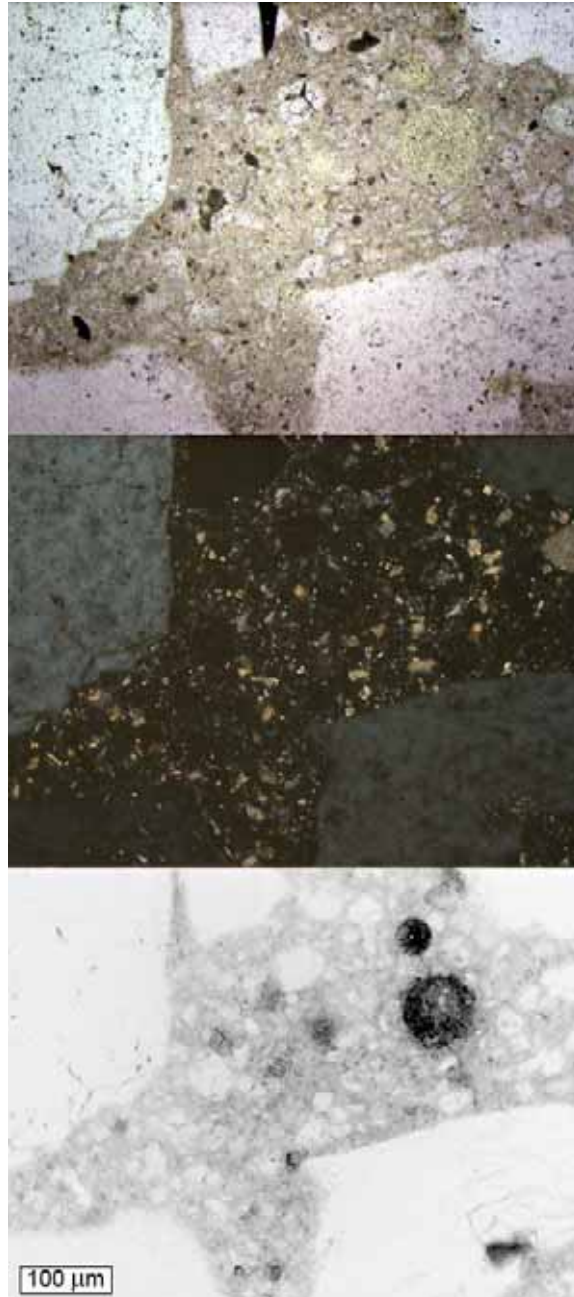


Figure 29: Carbonate dust in cement paste fraction in thin section prepared from core from US23, Section 19, away from joint, MTU ID US23-03. From top to bottom: transmitted light, crossed-polars, and epifluorescent mode images.

THIS PAGE INTENTIONALLY LEFT BLANK

SB US-23, MDOT Aggregate Test Site Section B

This site was selected because it did not exhibit MRD, and could be used as a basis for comparison with the newer JPCP sites that did exhibit MRD. Of particular interest was the condition of the ASR susceptible chert fraction of the fine aggregate. The site is pictured in Figures 30 and 31. Two core specimens were obtained, one core taken at a joint and another taken mid-panel. The sample from the joint was missing a portion of the core as shown in Figure 32. The core from mid-panel had a branched crack running through the entire depth of the core, as shown in Figure 33. Slight alkali-silica reactivity was observed by the staining method, and was limited to chert fine aggregate particles. Only a few of the reactive fine aggregate particles showed evidence of cracking, an example of which is shown in Figure 34. The isolated instances of ASR related cracks at this site were in contrast to the extensive inter-connected crack networks between chert particles observed in the other newer JPCP sites (M-59 and I-696). An overview of the slab stained with sodium cobaltinitrite is included in Figure 34. The air-void parameters, summarized in Table 5, were adequate for freeze-thaw protection. Results of equivalent w/c ratio measurements are included in Table 4. Figure 35 shows fly ash in a petrographic microscope image from the cement paste.



Figure 30: Overview of US-23, Section B test site.



Figure 31: Deteriorated crack from US-23, Section B test site.

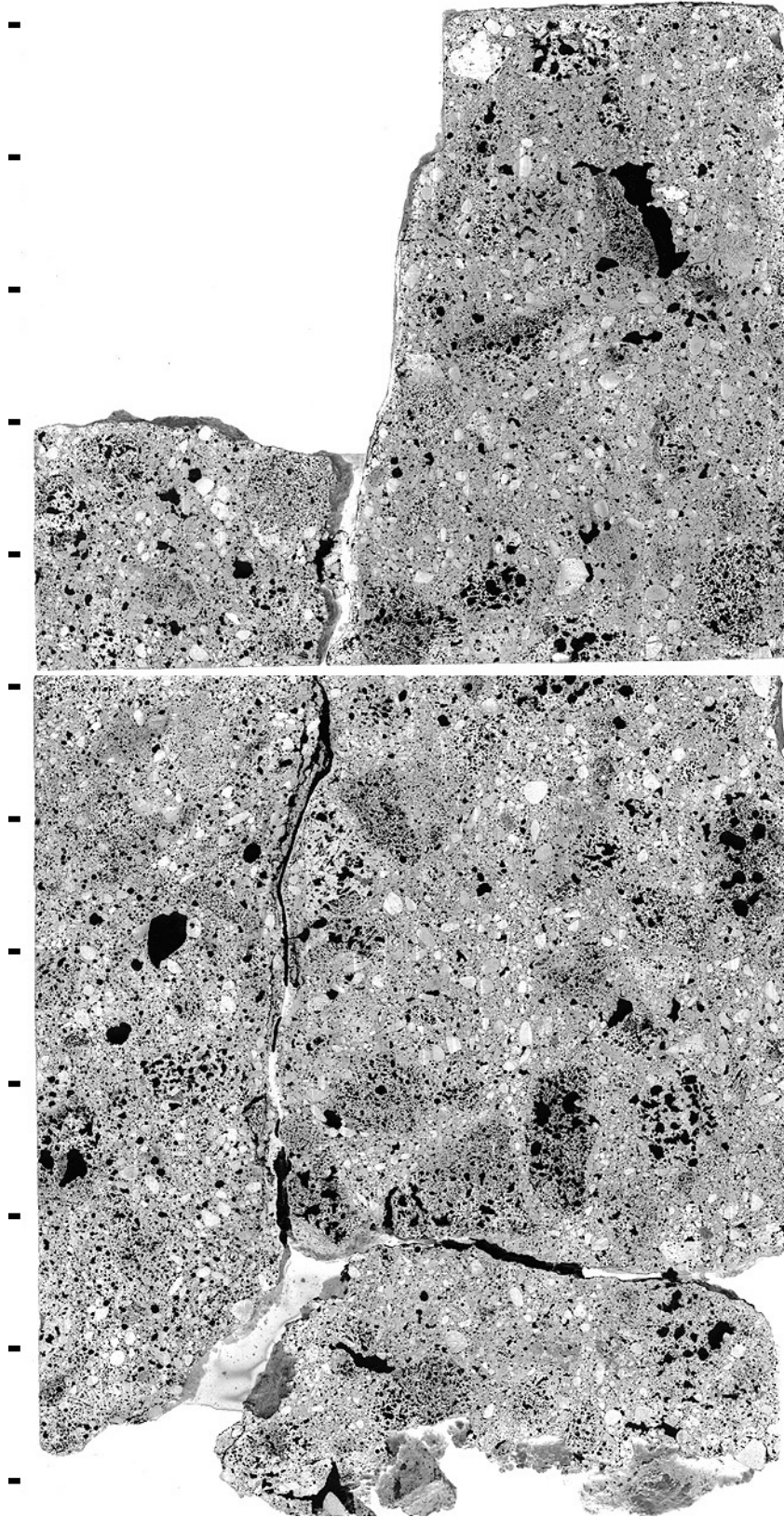


Figure 32: Polished slabs to represent cross-section through core MTU US23-07.

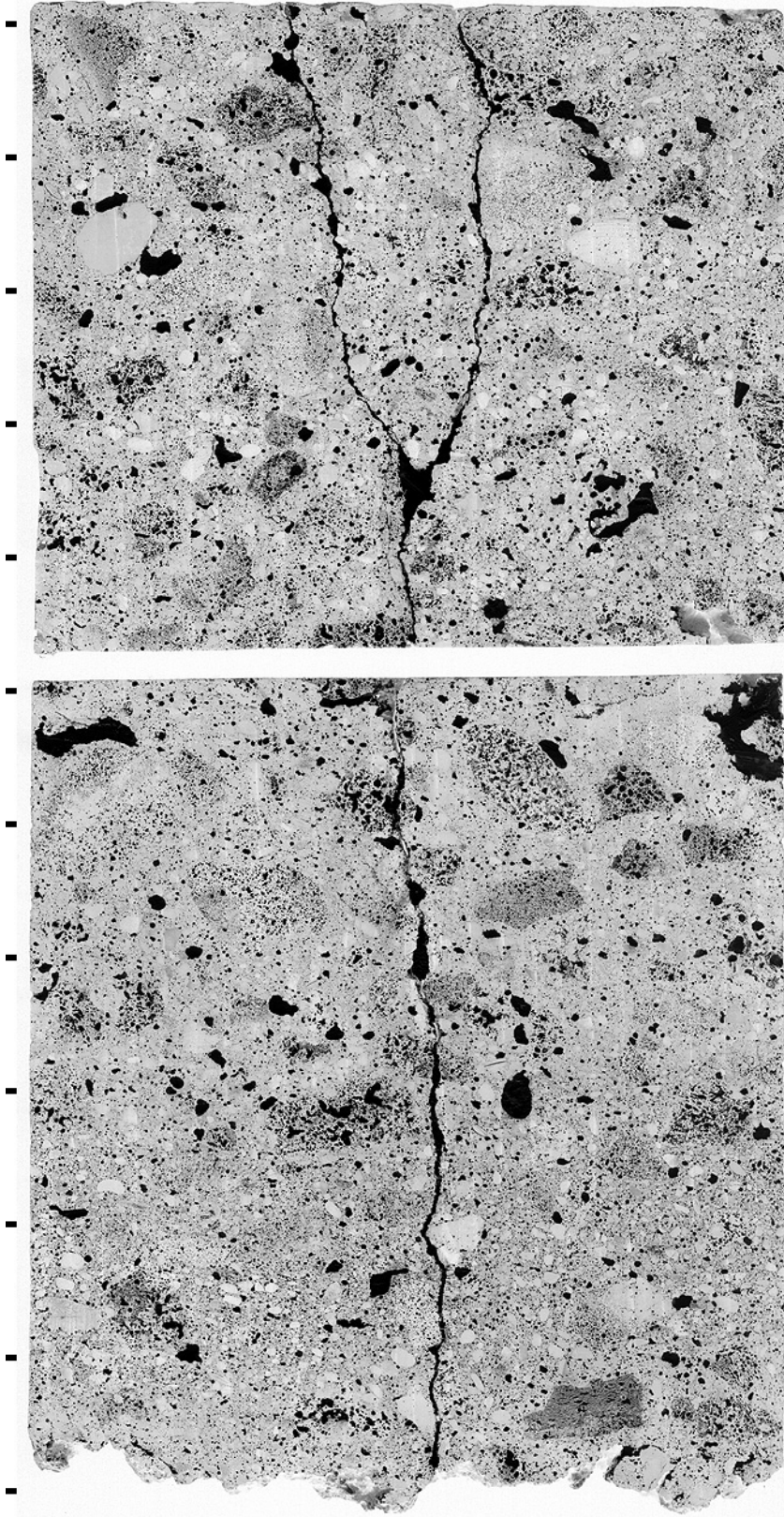


Figure 33: Polished slabs to represent cross-section through core MTU US23-06.

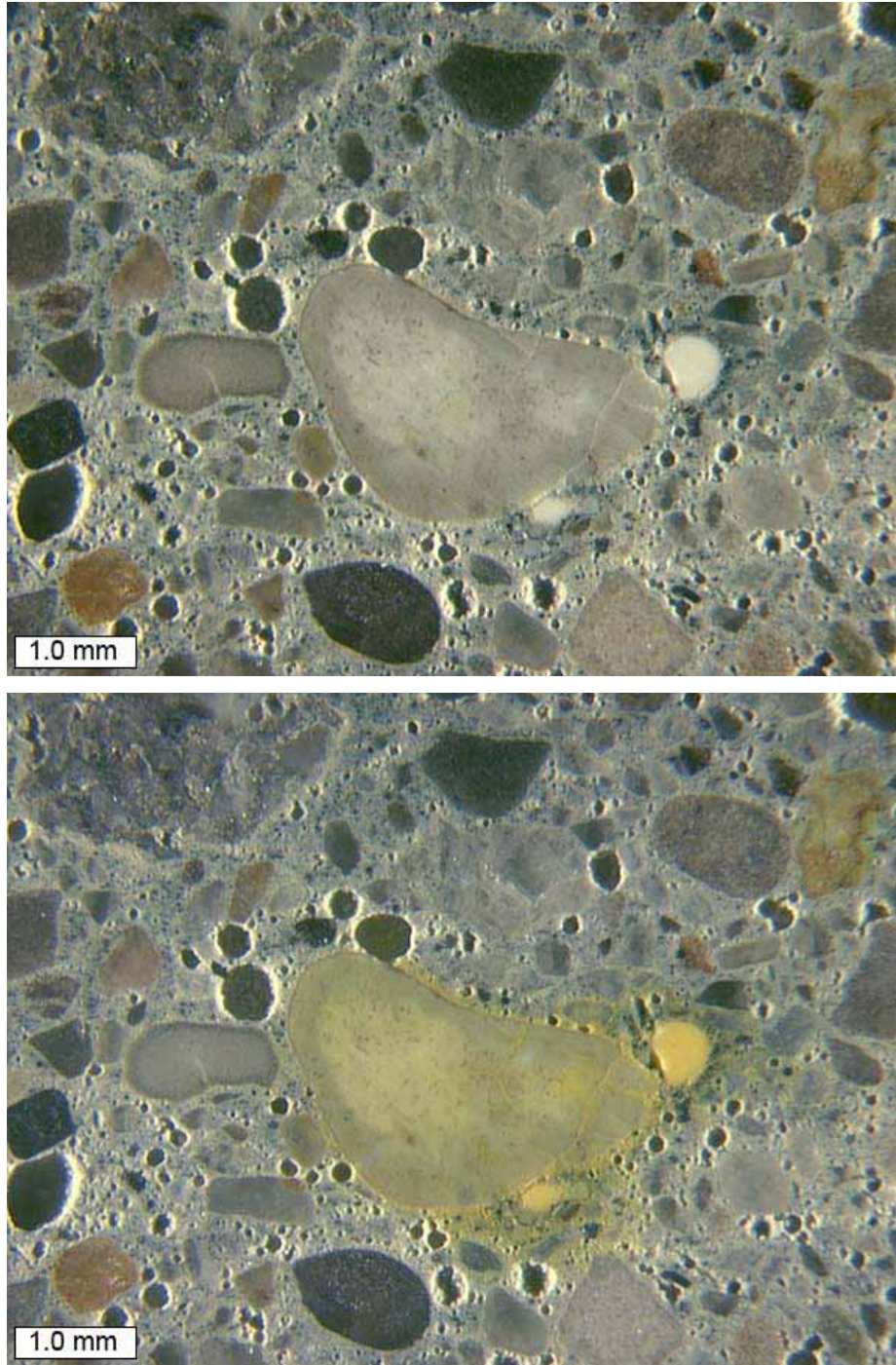


Figure 34: Alkali silica reaction in fine aggregate and associated cracking, before and after sodium cobaltinitrite stain, polished slab from top half of US-23, Section B, mid-panel, MTU ID US23-06.

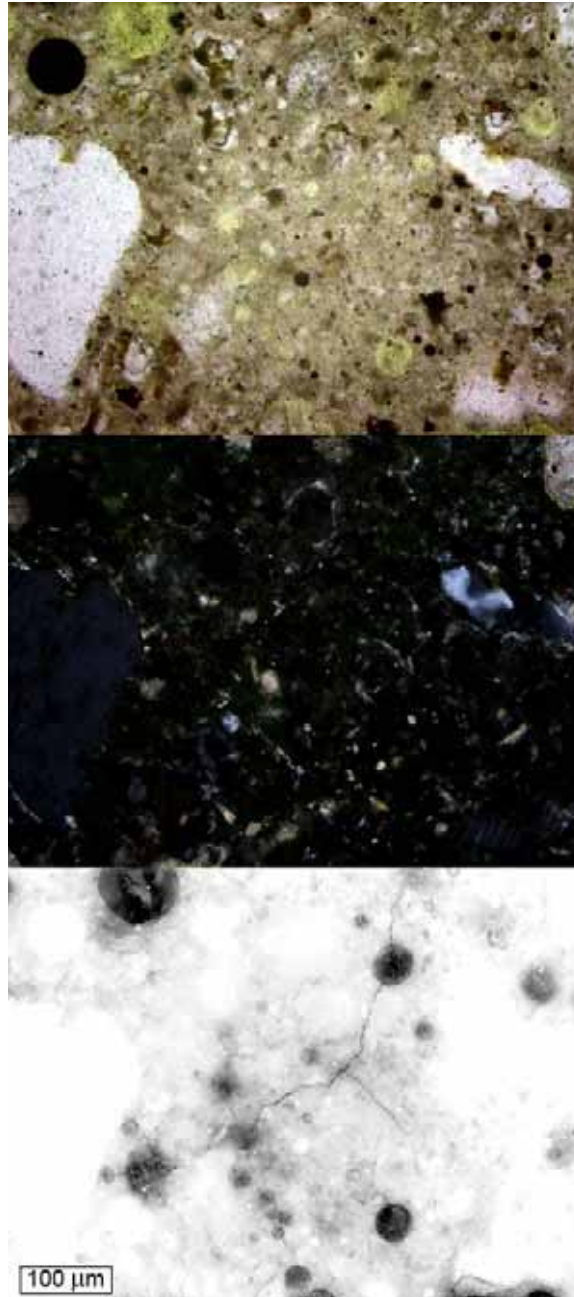


Figure 35: Fly ash in cement paste fraction in thin section prepared from core from US23, Section B at longitudinal joint, MTU ID US23-07. From top to bottom: transmitted light, crossed-polars, and epifluorescent mode images.

Summary

The results of the field investigation are summarized in Table 6. ASR has been implicated as a primary cause in two of the coring sites and possibly contributing to distress in another four sites. The next most common distress mechanism is a poor air-void system as judged by test results for spacing factor that exceeded the 0.2 mm threshold suggested in ASTM C 457.

The joint deterioration observed in one site (SB M-5, Novi) was not explainable solely using the data available, although the quality of the concrete made with fly ash was noted as being better than that made without fly ash, indicating a potential positive impact of using this supplementary cementitious material (SCM).

Table 6: Summary of distress mechanisms observed in test sites.

Core Site	Description	MTU ID	Primary Mechanism	Contributing Mechanism
WB I-696, I-94 interchange	1978	696-1	None observed	Borderline air-void system
	1995 median lane	696-8	ASR	Borderline air-void system
	1995 outside lane	696-11	ASR	Poorly distributed air-void system
SB M-5, 12 Mile Rd. to 14 Mile Rd.	Outside lane	M5-5	Unexplained joint distress	Minor ASR
	Median lane	M5-2		
EB M-59, Hayes Rd. to Romeo Plank Rd.	Outside lane	M59-2	ASR	
EB M-14, I-94 to Huron River	Outside lane	M14-3	Poor air-void system	Minor ASR
NB US-23, Sec. 19	Outside lane	US23-03	Poor air-void system and relatively high <i>w/c</i>	Minor ASR
SB US-23, Sec. B	Outside lane	US23-07	None observed	Minor ASR

THIS PAGE INTENTIONALLY LEFT BLANK

DISCUSSION AND CONCLUSIONS

Based upon previous research conducted by Michigan Tech for MDOT and the results of this study, the two distress mechanisms that are most frequently contributing to the observed distress are ASR and paste freeze-thaw damage. Issues related to paste freeze-thaw are already under investigation by Michigan Tech under a separate contract with the MDOT. Thus, the proposed research plan focuses exclusively on mitigating the aforementioned identified ASR problem. As a supplement to facilitate understanding of the issues pertinent to ASR, a review of ASR and relevant mitigation practices is provided here.

It is common knowledge that fresh concrete is extremely caustic and can cause serious burns if left in prolonged contact with skin. The pore fluids present in hardened concrete are just as caustic, but pose no danger, since the volumes of the fluid are so low, and the permeability of concrete is so low, that on a freshly fractured surface there is insufficient fluid available to harm the skin. But for silicon-oxygen bonds, such as those present in aggregates or SCMs embedded in the concrete, it is a different story.

Concrete pore fluids are caustic due the high concentration of hydroxyl anions (OH^-). These OH^- anions attack the silicon-oxygen bonds of aggregates as well as the silicon-oxygen bonds of SCMs (such as the glassy silico-aluminate phases present in fly ash and GGBFS). Since pore fluids maintain electrical equilibrium, any OH^- anions present are balanced by cations. In the pore fluids of hardened concrete, the most abundant cations are generally K^+ , and Na^+ . Concentrations of Ca^{2+} , another important cation, are relatively lower, since Ca^{2+} cations preferentially precipitate out into solid phases such as portlandite [$\text{Ca}(\text{OH})_2$] or the calcium silicate hydrate phases that make up the bulk of the hardened cement paste.

Specifically, when alkalis are discussed in terms of portland cement systems, it is understood that potassium and sodium are the elements under consideration. Abundant alkalis translate directly into abundant OH^- anions in the pore solution; which has implications for the silicon-oxygen bonds as mentioned previously. When silicon-oxygen bonds are disrupted, the silica is free to form complex polymers incorporating further OH^- anions, cations, and water molecules. These alkali-silicate-hydrate polymers make up the familiar silica gels associated with ASR.

The susceptibility of silicon-oxygen bonds present in minerals and rocks to disruption by high OH^- concentration environments is generally a function of the available surface area and crystal imperfections. For relatively large single crystal quartz grains, such as those that make up the bulk of sand grains in Michigan, the silicon-oxygen bonds are for the most part unaffected by OH^- ion concentrations present in concrete pore fluids; while the silicon-oxygen bonds of sand grains composed of more porous microcrystalline quartz, such as chert, are readily attacked. Although not a major component, chert is present on the order of 3% to 10% according to historic MDOT records of lithographic counts of Michigan fine aggregate sources. Silicon-oxygen bonds of poorly crystalline materials, often characterized as glassy, are also readily attacked.

Initially, silica gels tend to be rich in sodium and potassium and capable of easily flowing through the capillary pores of hardened concrete. Over time, these fluid gels tend to incorporate more calcium, and become brittle and hard, much like the calcium silicate hydrate phases that give concrete its strength. However, in certain situations the incorporation of Ca^{2+} ions from the pore solution by silica gel, in combination with the continued abundance of K^+ , Na^+ , and OH^- ions in the pore solution, along with the continued presence of unreacted silicon-oxygen bonds in the aggregate, can lead to tensile stresses that exceed the strength of the concrete, leading to cracking and deterioration.

The key to ASR distress involves the formation of semi-permeable rims of rigid calcium-rich silica gels around the perimeters of reactive aggregate particles. Using chert as an example, silica gel formed at the surface of a chert sand particle is initially alkali-rich and fluid in nature. Over time, with continued contact with the pore solution, this fluid gel picks up calcium from the pore solution and becomes more rigid. This rigid membrane remains permeable, and allows pore solution to continue to pass into the chert particle. OH^- , K^+ , and Na^+ ions in the pore solution will continue to interact with remaining intact silicon-oxygen bonds within the chert, forming additional silica gel that can not escape the semi-permeable rigid membrane at the perimeter. In some cases, pressure builds within the chert sand particle until it cracks the surrounding concrete, as illustrated in Figures 10, 11, 14, 17, 19, 20, 22, 26-28, and 34. Figure 19 is especially interesting, as it shows two inert sand particles split in half by cracks emanating from surrounding reactive chert particles. Under the right conditions, when there is abundant reactive and expansive chert particles, cracks connect between chert particles, and disrupt the concrete with continuous crack planes, as shown in Figures 6, 7, 12, 13, and 21.

Alternatively, chert particles may also show signs of ASR, but without any associated cracking, as illustrated in Figures 23 and 24. In such cases, it is possible that there were insufficient Na^+ and K^+ cations and corresponding OH^- anions in the pore solution for the reaction to proceed to the point where cracking occurred.

The role of SCMs in the prevention of ASR is widely recognized. The combination of their very fine particle size, and poorly crystalline nature, allows for the rapid consumption of alkalis and hydroxyl ions present in the pore solution and formation of alkali silica hydrate gels; leaving fewer alkalis and hydroxyl ions to interact with reactive aggregates. Although these silica gels will also consume calcium and become more rigid, there is no danger of further reaction with the pore solution, as the silicon-oxygen bonds in the small SCM particles have already been completely consumed by the initial reactions. In spite of their beneficial aspects, SCMs can also in themselves act as a source of additional alkalis, and depending on their level of addition, exacerbate ASR.

RECOMMENDATIONS FOR IMPLEMENTATION & FURTHER RESEARCH

MDOT and the Michigan Concrete Paving Association (MCPA) are collaborating on a means to mitigate the ASR problem. Several local governmental agencies in southeastern Michigan have implemented the MCPA's *Concrete Pavement Durability Specification for Local Agencies* with regard to ASR mitigation. MDOT is monitoring the impacts and benefits of the specification. It is recognized that the recommendations described in MCPA document generally represent a conservative approach for mitigation of ASR that follows current national mitigation practice.

According to the specification, aggregates will be tested using the AMBT as specified in ASTM C 1260 *Standard Test Method for Potential Alkali Reactivity of Aggregates (Mortar-Bar Method)*. If the expansion of the mortar bars is less than 0.10% at 14 days, the aggregates shall be considered innocuous and there are no restrictions or ASR mitigation required. If the expansion exceeds 0.10% at 14 days, mitigation for ASR must be done using one of the following two methods:

- Method 1: Substitute a portion of the cement with fly ash, GGBFS Grade 100 or 120, or a ternary mix (blended cement) containing a blend of portland cement and slag cement, or fly ash, or silica fume. If a Class F fly ash is used the calcium oxide (CaO) content shall be less than 10% and the available alkalies shall not exceed a maximum of 1.5%. If a Class C fly ash is used, it must have a minimum total oxides ($\text{SiO}_2 + \text{Al}_2\text{O}_3 + \text{Fe}_2\text{O}_3$) of 66% and a minimum SiO_2 of 38%. ASTM C 1567 *Standard Test Method for Determining the Potential Alkali-Silica Reactivity of Combinations of Cementitious Materials and Aggregate (Accelerated Mortar-Bar Method)* using both the fine and coarse aggregate along with the proposed cementitious material for the concrete mixture will be conducted and the mitigation is acceptable if expansion is less than 0.10% at 14 days.
- Method 2: Use low-alkali cement (alkali content does not exceed 0.60% expressed as Na_2O equivalent) and maintain the total alkali content of the concrete from the cementitious materials at no more than 3.0 lbs/yd³ (Na_2O eq.). The total alkali contribution is calculated by the quantity contained in the portland cement only.

The approach described in Method 2 is applicable only in those situations where low-alkali cement is available. Limits on cement alkalinity will likely eliminate from consideration many of the cement sources currently available in Michigan. Method 2 does not allow for the use of SCMs, therefore computation of the total concrete alkali content is based solely on the contribution of the portland cement. Alkalies present in portland cement are generally in the form of soluble salts, which makes them readily available for participation in ASR. The approach described in Method 1 allows for the incorporation SCMs; specifically GGBFS, silica fume, and fly ash, but places restrictions on the maximum calcium and alkali contents of Type F fly ashes, and the minimum silicon, aluminum, and iron contents of Type C fly ashes. The alkalies in fly ash may be present as soluble salts, but may also be present in less-soluble phases such as within glasses or insoluble crystalline phases. For this reason, the provision makes an effort to place a limit on the amount of available alkalies, as measured by ASTM C 311 *Standard Test Methods*

for Sampling and Testing Fly Ash or Natural Pozzolans for Use in Portland-Cement Concrete.

The research team believes that the adoption of this approach is a good first step for MDOT to start addressing the ASR issue observed in the course of this and previous studies, yet the following issues still remain:

- Very few sources of Class F fly ash are available in southeastern Michigan and the available alkalis of these fly ashes are unknown. Further, this specification will eliminate from consideration many of the Class C fly ashes that are available.
- The current maximum limits for cement substitutions per MDOT specifications are: 40% GGBFS, 30% fly ash, 40% ternary (25% GGBFS and 15% fly ash). It is unknown how these limits contribute to the noted problem, if at all.
- Approval of aggregate sources and ASR mitigation is wholly dependent upon the results of the AMBT (ASTM C1260 for initial screening and ASTM C1567 for verification of mitigation using SCMs). The short-term results of this testing should be correlated with long-term testing using the CPT as described in ASTM C1293 - *Standard Test Method for Determination of Length Change of Concrete Due to Alkali-Silica Reaction*. The Contractor chooses whether to use a particular aggregate source or mitigate. An aggregate source is not necessarily approved or denied from ASTM C1260 results.
- Low alkali cements are not readily available in Michigan.
- Other than in very isolated cases, the ASR observed in Michigan pavements and structures has been attributed to chert and siltstone constituents within the fine aggregate. The presence of blast furnace slag coarse aggregate (and to some degree, Class C fly ash) appears to play a role in the observed distress, but this role remains undefined.

The findings from phase I confirm that additional research is needed to define the unique post-construction, interaction relationships that are occurring amongst commonly used Michigan materials for making pavement concrete to assure their selection produce a long-term, durable concrete mixture. These materials include fine aggregate susceptible to forming expansive ASR, blast furnace slag coarse aggregate, Class C fly ash, and high-alkali cements.

The proposed experimental approach was to follow the most recent protocols developed for the FHWA, using AMBT (ASTM C 1260 and 1567) and CPT (ASTM C 1293) to determine the quantify the nature of the ASR problem and to identify practical mitigation strategies that can be employed to minimize its occurrence in the future. Future work to better understand the geographical distribution of reactive constituents in fine aggregate sources is also recommended.

The joint deterioration observed that was not related to ASR was not explainable solely using the data available. It is recommended that this issue be studied separately under a smaller, focused forensic study that carefully evaluates the conditions that exist during construction and field exposure conditions (especially deicer chemicals) to determine what design and construction practices might be contributing to the formation of this distress.

THIS PAGE INTENTIONALLY LEFT BLANK

LIST OF ACRONYMS, ABBREVIATIONS AND SYMBOLS

ACR, alkali-carbonate reactivity
AMBT, Accelerated Mortar Bar Test
ASR, alkali-silica reactivity
ASTM, American Society for Testing and Materials
CPT, concrete prism test
FHWA, Federal Highway Administration
GGBFS, ground granulated blast furnace slag
JPCP, jointed plain concrete pavement
JRCP, jointed reinforced concrete pavement
PCC, portland cement concrete
MCPA, Michigan Concrete Paving Association
MDOT, Michigan Department of Transportation
MRD, Materials-related distress
MTU, Michigan Technological University
SCM, supplementary cementitious material
SHRP, Strategic Highway Research Program
w/c, water to cementitious ratio

THIS PAGE INTENTIONALLY LEFT BLANK

BIBLIOGRAPHY

American Concrete Institute (1998). "State-of-the-Art Report on Alkali-Aggregate Reactivity." *ACI Manual of Concrete Practice: Part 1*. ACI 221.1R-98. ISSN 0065-7875. American Concrete Institute, Farmington Hills, MI.

Dolar-Mantuani, L. (1982). *Handbook of Concrete Aggregates: A Petrographic and Technological Evaluation*. Noyes Publications. Park Ridge, New Jersey.

Farney, J.A., Kosmatka, S.H., (1997). *Diagnosis and Control of Alkali-Aggregate Reactions in Concrete*. Concrete Information Series No. IS413.01T. Portland Cement Association. Skokie, IL. ISBN 0 89312 146 0.

Folliard, K., Fournier, B., Thomas, M., (2007). *ASR Testing and Evaluation Protocols, Protocol A: Determining the Reactivity of Concrete Aggregates and Selecting Appropriate Measures for Preventing Deleterious Expansion in Concrete*. Prepared for the Federal Highway Administration by Transtec.

Helmuth, R. (1993). *Alkali-Silica Reactivity: An Overview of Research*. SHRP-C-342, Strategic Highway Research Program, Washington, DC.

Ichikawa, T., Miura, M. (2007) "Modified Model of Alkali-Silica Reaction" *Cement and Concrete Research*, Vol. 37, pp. 1291-1297.

Malvar, L.J., and Lenke, L.R., (2006) "Efficiency of Fly Ash in Mitigating Alkali-Silica Reaction Based on Chemical Composition" *ACI Materials Journal*, Vol. 103, No. 5, pp. 319-326.

Neville, A. M. (1996). *Properties of Concrete*. John Wiley and Sons, Inc., New York, New York.

Shehata, M.H., Thomas, M.D.A., Bleszynski, R.F., (1999) "The Effects of Fly Ash Composition on the Chemistry of Pore Solution in Hydrated Cement Pastes" *Cement and Concrete Research*, Vol. 29, pp. 1915-1920.

Shehata, M.H., Thomas, M.D.A., (2000) "The Effects of Fly Ash Composition on the Expansion of Concrete Due to Alkali-Silica Reaction" *Cement and Concrete Research*, Vol. 30, pp. 1063-1072.

Shehata, M.H., Thomas, M.D.A., (2006) "Alkali Release Characteristics of Blended Cements" *Cement and Concrete Research*, Vol. 36, pp. 1166-1175.

Stark, D. (1991). *Handbook for the Identification of Alkali-Silica Reactivity in Highway Structures*. SHRP-C/FR-91-101. Strategic Highway Research Program, Washington, DC.

Stark, D. (1994). *Alkali Silica Reactions in Concrete*. Significance of Tests and Properties of Concrete and Concrete-Making Materials. STP 169C. American Society for Testing and Materials. Publication Code Number 04-169030-07. Philadelphia, PA. pp. 365-371.

Van Dam, T. J., Sutter, L. L., Smith, K. D., Wade, M., Peterson, K.R., (2002). *Guidelines for Detection, Analysis, and Treatment of Materials-Related Distress in Concrete Pavements - Volume 2: Guidelines Description and Use*, FHWA-RD-01-163, Washington, DC.

THIS PAGE INTENTIONALLY LEFT BLANK

APPENDIX

The following appendix materials are available in portable document format (PDF) on compact disk (CD):

- Appendix A, I-696 Core Site.
- Appendix B, M-5 Core Site.
- Appendix C, M-59 Core Site.
- Appendix D, M-14 Core Site.
- Appendix E, US-23 SHRP Section 19 Core Site.
- Appendix F, US-23 MDOT Aggregate Test Road Section B Core Site.
- Appendix G, Description of w/c ratio determination methodology.